# Dynamics of Surf-Zone Turbulence in a Spilling Wave

by

Francis C. K. Ting

and

James T. Kirby

RESEARCH REPORT NO. CACR-95-11

July, 1995

Center for Applied Coastal Research
Ocean Engineering Laboratory
University of Delaware
Newark, DE 19716

# Dynamics of surf-zone turbulence in a spilling breaker

**Francis C. K. Ting** [a], **James T. Kirby** [b]

[a] *Texas Transportation Institute, Texas A&M University, College Station, TX 77843-3135, USA*

[b] *Center for Applied Coastal Research, Department of Civil Engineering, University of Delaware, Newark, DE 19716, USA*

**Abstract**

The structure of turbulence in a spilling breaker has been studied experimentally based on the transport equation for turbulent kinetic energy (the $k$-equation). We study turbulence transport in the evolving flow from the breaking point to the inner surf zone in the region below trough level and above the bottom boundary layer. The study shows that turbulence transport processes are similar in the outer and inner surf zones. It is found that diffusive transport plays the most important role in the distribution of turbulence, while advection is important mainly near the surface. It is also found that although turbulence production below trough level amounts to only a small portion of the wave energy loss, the production term is not small compared to the dissipation term and the major terms in the $k$-equation and thus it cannot be neglected. The mixing length is estimated based on the measured rates of vertical advance of the turbulent front, and comparisons of turbulence production and energy dissipation. The results are similar to those found in previous studies . It is shown that the length scale and velocity scale of the large eddies are subject to turbulence transport processes, therefore their distributions cannot be prescribed in an easy way. The relative values of the components of the Reynolds stress tensor are examined. The results of analysis supports the notion that surf-zone turbulence created by spilling and plunging breakers differ primarily in the method of en-

ergy transfer from organized wave-induced motion to turbulent motion, and the constraints imposed by the mean flow and the solid bottom on the large-scale turbulence.

---

## 1. Introduction

Wave breaking plays an important role in sediment transport and beach profile change. In the surf zone, turbulence generated by broken waves causes wide-spread and intense sediment suspension. Turbulence carries sediment away from the bed, making it available for transport by waves and wave-induced currents. Prediction of sediment transport requires modeling of the distributions of fluid velocities and suspended sediment concentrations. The transport equation for suspended sediment is given by

$$\frac{\partial \tilde{c}}{\partial t} + \frac{\partial \tilde{u}_j \tilde{c}}{\partial x_j} = -\frac{\partial \widetilde{u_j' c'}}{\partial x_j} + w_f \frac{\partial \tilde{c}}{\partial z} \tag{1}$$

In Eq. 1, the tilde is an operator to take an ensemble average, $x_j$ ($j = 1, 2, 3; x_1 = x, x_2 = y, x_3 = z$) are the coordinates of a Cartesian frame with $z$ extending positive upward from the undisturbed water surface, $\tilde{u}_j$ ($j = 1, 2, 3; \tilde{u}_1 = \tilde{u}, \tilde{u}_2 = \tilde{v}, \tilde{u}_3 = \tilde{w}$) are the components of the ensemble-averaged water particle velocity, $\tilde{c}$ is the ensemble-averaged sediment concentration, $u_j'$ and $c'$ are the fluctuating parts of velocity components and sediment concentration, and $w_f$ is the sediment fall velocity. The ensemble-averaged velocity $\tilde{u}_j$ is the organized wave-induced velocity which includes both the undertow and the orbital wave motion; it may be found by solving the momentum equations. In regular waves, periodic motion allows the ensemble-averaged velocities to be obtained by phase-averaging the measured velocities over successive waves.

Eq. 1 can be solved only if the turbulent transport $\widetilde{u_j' c'}$ can be determined in some way. In direct analogy to turbulent momentum transport, turbulent

mass transport is often assumed to be related to the gradient of the transported quantity, i.e.

$$-\widetilde{u_j' c'} = D\frac{\partial \tilde{c}}{\partial x_j} \tag{2}$$

where $D$ is the turbulent diffusion coefficient. In the eddy-diffusivity concept, the turbulent diffusion coefficient is proportional to a velocity scale and a length scale, i.e.

$$D = l\sqrt{k} \tag{3}$$

where $l$ is the length scale of the large eddies, and $k$ is the turbulent kinetic energy defined by

$$k = \frac{1}{2}\widetilde{u_i' u_i'} \tag{4}$$

In the one-equation model $l$ is specified and $k$ is found by solving the energy equation for the turbulence (the $k$-equation). For high Reynolds numbers, the $k$-equation can be written

$$\frac{\partial k}{\partial t} + \frac{\partial \tilde{u}_j k}{\partial x_j} = -\frac{\partial}{\partial x_j}\left(\frac{1}{\rho}\widetilde{u_j' p'} + \widetilde{u_j' k'}\right) - \widetilde{u_i' u_j'} S_{ij} - 2\nu \widetilde{s_{ij} s_{ij}} \tag{5}$$

where $p'$ is the fluctuating part of pressure, $\rho$ is the density, $\nu$ is the kinematic viscosity, $k'$ is the instantaneous value of $k$ given by

$$k' = \frac{1}{2}u_i' u_i' \tag{6}$$

and $S_{ij}$, $s_{ij}$ are the mean rate of strain and fluctuating rate of strain respectively

$$S_{ij} = \frac{1}{2}\left(\frac{\partial \tilde{u}_i}{\partial x_j} + \frac{\partial \tilde{u}_j}{\partial x_i}\right), \qquad s_{ij} = \frac{1}{2}\left(\frac{\partial u_i'}{\partial x_j} + \frac{\partial u_j'}{\partial x_i}\right) \tag{7}$$

Eq. 5 states that the local time rate change of turbulent kinetic energy is due to convection by mean flow, diffusive transport by pressure and turbulent fluctuations, turbulent energy production, and viscous dissipation. The relative

importance of these terms are important in turbulence modeling and must be determined.

Many researchers have studied turbulence in breaking waves before, with the main effort centered on laboratory experiments. Some of the more detailed studies include Stive (1980), Nadaoka and Kondoh (1982), Stive and Wind (1982), Sakai et al. (1982, 1984), Hattori and Aono (1985), Nadaoka (1986), Mizuguchi (1986), Okayasu et al. (1986) and Nadaoka et al. (1989). So far, the velocity field in the surf zone has been relatively well studied, but the dynamics of turbulence has not. To date, turbulence transport in the surf zone has not been studied in a systematic manner. For example, it is believed that the main part of turbulence production takes place above the trough level, and spreading of turbulent energy is due to convection (Peregrine and Svendsen, 1978). Because of this, production below the trough level is often neglected in turbulence modeling. It is thought that only a small portion of the wave energy loss is dissipated below the trough level (Svendsen, 1987a). There are also much ambiguity in the determination of the length and velocity scales of surf-zone turbulence. The difficulty arises because the dynamical role of individual transport processes such as advection, diffusion, production and dissipation are poorly understood. In order to model turbulent flows we must first understand the turbulence transport processes.

Recently, Ting and Kirby (1994) have studied the characteristics of undertow and turbulence in spilling versus plunging breakers. They found that turbulent kinetic energy is transported seaward under a spilling breaker and landward under a plunging breaker below the trough level. They concluded that turbulence transport processes are different in spilling and plunging breakers, and suggested that further work on this topic is warranted. Since the transport equations for

suspended sediment and turbulent kinetic energy are coupled, a thorough understanding of turbulence transport would be important for developing working models of coastal processes. The dynamics of turbulence in a strong plunging breaker has been studied by Ting and Kirby (1995) based on the transport equation for turbulent kinetic energy. They found that turbulence transport under a strong plunging breaker is dominated by large-scale motions that can be related to the wave characteristics. It was also found that advective and diffusive transport of turbulence are important, thus they cannot be neglected in turbulence modeling.

This present study deals with the dynamics of surf-zone turbulence created by a spilling breaker on a plane beach. Experiments were conducted in a two-dimensional wave tank where water particle velocities were measured using a fibre-optic laser-Doppler anemometer and surface elevations were measured using a capacitance wave gage; the measurements were obtained at several stations inside and outside the surf zone. Based on the measured data, we study the process of turbulence transport in the evolving flow within the surf zone. We first present the experimental results and discuss how the organized wave-induced motion (mean flow) and the turbulent velocity fluctuations transport turbulent kinetic energy; then, we investigate the relative importance of the terms in the $k$-equation. In order to give an overall picture of the dynamical role of turbulence in spilling breakers, earlier published results are discussed and the question of how the dynamics of turbulence differs between spilling and plunging breakers is explained.

## 2. Experimental equipment and procedures

The measurements from which the present results are derived were partly

used in a previous study (Ting and Kirby, 1994). To prevent duplication of the description of details just a brief account of the experimental equipment and procedure is given below.

The experiments were conducted in a two-dimensional wave tank in the Ocean Engineering Laboratory at University of Delaware. The wave tank was 40 m long, 0.6 m wide and 1.0 m deep. Cnoidal waves were generated in a water depth of 0.4 m by a bulkhead wave generator. The wave height was 12.5 cm in the constant-depth section, and the wave period was 2.0 s. The ratio of deep-water wave height $H_0$ to deep-water wavelength $L_0$ was 0.020 based on linear shoaling. The waves broke in the form of a spilling breaker on a 1 on 35 sloped false bottom built of marine plywood.

A schematic diagram of the experimental arrangement and the coordinate system is shown in Fig. 1. The following notations are used in this paper: $\zeta =$ instantaneous water surface elevation, $\overline{\zeta} =$ mean water surface elevation, $d =$ local still water depth, $h = d + \overline{\zeta} =$ local mean water depth, and the subscript $b$ denotes the breaking point. The latter is defined as the location where air bubbles begin to be entrained in the wave crest.

Water surface elevations and velocities were measured at eight locations along the centerline of the wave tank (six of these locations were inside the surf zone); their exact locations and water depths are given in Table 1. The horizontal distance covered by the measuring section within the surf zone was 3.06 m, extending from $d = 18.5$ cm near the breaking point to $d = 9.7$ cm in the inner surf zone. Water particle velocities were measured using a fibre-optic laser-Doppler anemometer (LDA). Velocity measurements were conducted mainly in the region below trough level and above the bottom boundary layer.

Unfortunately, the blue line of the laser did not have sufficient power therefore horizontal and vertical components of water-particle velocity were measured using the green line of the laser by conducting the same experiment twice. Data were acquired using an IBM PS/2 Model 30 286 computer equipped with a MetraByte DASH-16(F) data acquisition board. The sampling frequency was 100 Hz for each channel and the sampling time was 204.8 s. The wave gage and the fibre-optic probe were mounted on an instrument carriage which could slide along the top of the tank on two rails. The probe was submerged in water during experiment.

The organized wave-induced velocity was obtained by phase-averaging the instantaneous velocity over one hundred and two successive waves; the deviations from the phase average were considered to be turbulent velocity fluctuations. Visual observations showed that the foam was confined to a region near the crest of the broken waves, but air bubbles were entrained and transported to the bottom by sporadic, three-dimensional vortices descending obliquely downward. When air bubbles passed through the probe volume of the LDA signal drop-out occurred and the Doppler frequency was held at the last measured value. This resulted in spurious signals which were partly recorded as turbulence. In order to minimize the influence of aeration on the velocity measurements, data that were obtained during signal drop-out were not used in data analysis. It was shown in Ting and Kirby (1994) that we have sampled sufficient realizations to obtain stable wave and turbulence statistics. For the detailed experimental procedure the interested reader is referred to Ting and Kirby (1994).

## 3. Results and discussions

### *3.1. Turbulence transport*

Fig. 2 plots the phase-averaged water surface elevations at several stations in the surf zone. The temporal variations of quantities in this figure, and others to follow, are synchronized with the motion of the wave plate to show the phase relationship between different measuring points. Previous studies have shown that the height of the broken waves remains an approximate fixed proportion of the mean water depth in the inner surf zone (see Svendsen et al., 1978). This observation is used here to distinguish the outer surf zone from the inner surf zone. It is seen in Fig. 2 that the wave height to water depth ratio $H/h$ is slowing decreasing and the shape of the broken wave is almost constant shoreward of $(x - x_b)/h_b = 7.462$. Hence, this station may be considered to be the starting point of the inner surf zone.

Fig. 3 presents the results for $(x - x_b)/h_b = 4.397$, $h/h_b = 0.879$. Local wave height is 12.04 cm, wave set-up is 0.59 cm, mean water depth is 17.49 cm, and wave height to water depth ratio is 0.688. Phase-averaged horizontal and vertical velocities are plotted in Figs. 3a and 3b. All velocities are normalized by the wave celerity $C = \sqrt{gh}$. Trough level is located at $(z - \overline{\zeta})/h \approx -0.20$. Since the water surface elevation in the surf zone varies considerably from wave to wave, the trough level is defined as the highest point where the probe is submerged over the entire data run. The velocities presented in this paper are for the region below trough level and above the bottom boundary layer. Phase-averaged turbulent velocities are presented in Figs. 3c and 3d. In the outer surf zone the flow is evolving and turbulence is weak (cf. Figs. 4c and 4d). It is inferred from the temporal variations of turbulent velocities that the dissipation

rate is slow in the spilling breaker and thus turbulent energy does not die out between breakers but is more uniform in time. It may be observed that turbulent velocities are highest in the crest portion of the wave near the surface, but the peak gradually shifts to the trough portion of the wave as the distance from the surface increases. This trend is more distinct in the inner surf zone and has been observed in previous studies. It indicates that turbulent kinetic energy is generated in the wave crest and spread to the bottom, and the vertical mixing is slow. It is seen that the $u'$ component generally has more energy than the $w'$ component, which is to be expected.

Transport of turbulent kinetic energy by mean flow are presented in Figs. 3e and 3f. Because the transverse velocity component was not measured, turbulent kinetic energy is estimated by $k = (1.33/2)\left(\widetilde{u'^2} + \widetilde{w'^2}\right)$ after Stive and Wind (1982) and Svendsen (1987a). This assumes that the turbulent velocities resemble that in a plane wake, which has not been proven. However, Svendsen (1987a) has shown that the ratio $k/\left(\widetilde{u'^2} + \widetilde{w'^2}\right)$ does not vary greatly for a number of different shear flows hence the errors associated with this estimation is expected to be small. Fig. 3e shows that transport of turbulent kinetic energy by mean flow is predominantly seawards near the bottom. This phenomenon is observed in the outer surf zone as well as the inner surf zone (water particle velocities were not measured in the swash zone). The implications for coastal sediment transport were discussed in Ting and Kirby (1994). Transport of turbulent kinetic energy by turbulent velocity fluctuations are presented in Figs. 3g and 3h. Only the $u'^3$ and $w'^3$ components are shown since we did not measure $u'$ and $w'$ simultaneously. It is seen that $\widetilde{w'^3}$ is negative, which indicates that turbulence is spread downward by turbulence.

Fig. 4 presents the results for $(x - x_b)/h_b = 7.462$, $h/h_b = 0.809$. Local

wave height is 8.865 cm, wave set-up is 0.76 cm, mean water depth is 0.161 m, and wave height to wave depth ratio is 0.551. Phase-averaged horizontal and vertical velocities are plotted in Figs. 4a and 4b. Trough level is located at $(z - \overline{\zeta})/h \approx -0.20$. Phase-averaged turbulent velocities are plotted in Figs. 4c and 4d. These plots give evidence for existence of coherent structures in the spilling breaker. Nadaoka et al. (1989) have observed that wave breaking produces horizontal vortices in the spanwise direction, which then break down through the formation of vortices extending obliquely downward. These obliquely descending vortices are identifiable for only a short time, and similar but not identical vortices occur repeatedly in successive breakers. Since the LDA measures fluid velocities at only one point in space at a time, and the measured velocities are phase-averaged over many waves, they cannot provide detailed information on the spatial structure of the vortices and their evolution in time. However, the close resemblence of turbulent velocity fluctuations at different elevations indicates that there must be a high degree of organization in the turbulent motion, and the phase shift indicates that turbulent motion spreads slowly into the ambient flow. The rate of vertical advance of the turbulent front can be estimated from the time delay of the observed increase in turbulent velocity with depth. From Fig. 4d, the rate is about $0.4C$ from the time delay between the increase in turbulent velocity at $(z - \overline{\zeta})/h = -0.2957$ and $-0.4820$, $0.4C$ from $(z - \overline{\zeta})/h = -0.4820$ and$-0.6683$ and $0.3C$ from $(z - \overline{\zeta})/h = -0.6683$ and $-0.8857$. This time delay is partly caused by advective transport in a shear flow with mean velocity gradient $\partial\tilde{u}/\partial z$. From Fig. 4a, we estimate that the effect of shearing should not exceed $0.05C$. The modified velocity of 0.25–$0.35C$ is still considerably larger than the measured turbulent fluctuations. It is found that the variation of mixing rate over depth is small, whereas turbulent

velocity fluctuations decrease with distance from the surface. These observations suggest that the calculated turbulent diffusion coefficient could be too low at some depth if the length scale is held fixed and the velocity scale is taken to be the r.m.s. turbulent velocity fluctuations. Previously, Deigaard et al. (1986) have calculated distribution of turbulent kinetic energy in the inner surf zone by solving the linearized $k$-equation. They estimated the turbulent diffusion coefficient using Eq. 3 with $l = 0.07h$. Svendsen (1987a,b) pointed out that the calculated turbulent energy and its variation over depth were significantly larger than the measured values derived from Stive and Wind's measurements. Tada et al. (1990) included the vertical convection term in the $k$-equation but found that the effect of this on the vertical distribution of turbulent kinetic energy was small. However, they found that multiplying the production term by 0.3 and the dissipation term by 0.5 gave results that compared well with experiment. The reduction in the production by a factor of 0.3 was already proposed in the closure of Deigaard et al. (1987). The sensitivity of their model to variations in the production and length scale is given in Deigaard et al. (1991), which also contains a comparison between measured and simulated vertical distributions of turbulence.

The major weakness of the one-equation model is that the specification of length-scale distribution is rather arbitrary. In simple flows such as mixing layers, jets and wakes, the mixing length $l$ can be assumed constant across the shear layer and proportional to the local layer width $\delta$. For example, the value of $l/\delta$ is 0.07 in plane mixing layer, 0.09 in plane jet and 0.16 in plane wake (Rodi, 1984). Svendsen (1987a,b) proposed $l \sim 0.2$–$0.3h$ in breaking waves based on comparisons of computed and measured undertow velocity profiles. A more direct determination of $l$ is to measure the rate of spreading of turbulence

patches. The time for turbulence to spread throughout the water column is (see Ting and Kirby, 1995)

$$t \approx 0.4\frac{h^2}{D} \tag{8}$$

This must be equal to the observed mixing time

$$t_m \approx \frac{h}{\hat{u}} \tag{9}$$

where $\hat{u}$ is the velocity for vertical advance of turbulent front. Equating $t$ with $t_m$ and after using Eq. 3, we obtain

$$\frac{l}{h} \approx 0.4\frac{\hat{u}}{\sqrt{k}} \tag{10}$$

From Figs. 4c and 4d we find that $\sqrt{k} \sim 0.12C$ under the wave crest. Since $\hat{u}$ lies in the range of $0.25C$ to $0.35C$, Eq. 10 yields $l \sim h$. This is too large. However, the coefficient of 0.4 in Eq. 8 is for "fully mixed" condition. We expect that the turbulent front will not take that much time to reach the bottom. Keeping this in mind, the length scale of $l \sim 0.2$–$0.3h$ proposed by Svendsen (1987a,b) is more realistic. It appears that the length scale in breaking waves is somewhat larger than those in simple shear flows.

Transport of turbulent kinetic energy by mean flow and turbulent velocity fluctuations are shown in Figs. 4e–4h. Transport of turbulent energy by advection is upwards under the wave front and downwards under the back face of the wave. Transport of turbulent energy by turbulent fluctuations is equal to $\widetilde{u'k'}$ in the horizontal direction and $\widetilde{w'k'}$ in the vertical direction, where $k' = \frac{1}{2}(u'^2 + v'^2 + w'^2)$ is the instantaneous value of turbulent kinetic energy. We have measured $\widetilde{u'^3}$ and $\widetilde{w'^3}$ only, but the other components may be expected to behave in a similar manner. It is seen that $\widetilde{u'^3}$ is positive and $\widetilde{w'^3}$ is negative.

Hence, turbulent kinetic energy is transported shoreward by turbulent fluctuations while spreading downward. These measurements are consistent with visual observations of large-scale motions in breaking waves.

Fig. 5 presents the experimental results for $(x - x_b)/h_b = 10.528$, $h/h_b = 0.744$. Local wave height is 8.223 cm, wave set-up is 1.05 cm, mean water depth is 14.8 cm, and wave height to water depth ratio is 0.556. Comparing Fig. 5 to Fig. 3, it is seen that the structure of turbulence has many similarities in the outer and inner surf zones. This is different from plunging breakers where the structure of turbulence changes considerably from the outer surf zone to the inner surf zone (see Ting and Kirby, 1995). For the spilling breaker, wave breaking is confined to a region near the wave crest and the rate of energy transfer from wave to turbulence is relatively slow. Because of this, the size of the largest eddies is still smaller than the local water depth and thus the effect of the solid bottom on the eddy motion is small. These conditions allow the turbulent flow to evolve slowly under its own evolutionary tendencies. The rate of energy supply to turbulent motion is important in determining the turbulence structure because turbulent diffusion and dissipation are passive processes that can only proceed at a rate dictated by the behaviour of the large eddies. The rate of energy supply to the large eddies is of order $U^3/l$, where $l$ and $U$ are the length scale and velocity scale of the large eddies. The rate of energy supply is much higher in plunging breakers than in spilling breakers and consequently plunging breakers have large length and velocity scales. It could be argued that spilling and plunging breakers differ primarily in the method of energy supply to the turbulent motion, and the effects of the mean flow and the solid boundary on the large-scale turbulence; this will be discussed more fully later.

From Figs. 5a and 5d, we estimate that the rate of vertical diffusion is about

0.15–0.25$C$. It is seen that the rate of vertical mixing decreases shoreward. Considering that the source of energy for the large eddies is the available kinetic and potential energy released by wave breaking, we should expect that the length and velocity scales of the large eddies, and the mixing rate, will decrease with the wave height, that is, shoreward.

Further inshore, the broken waves have developed into a turbulent bore. Fig. 6 presents the experimental results for $(x - x_b)/h_b = 13.618$, $h/h_b = 0.668$. Local wave height is 7.52 cm, wave set-up is 1.29 cm, mean water depth is 13.3 cm, and wave height to water depth ratio is 0.565. Fig. 7 presents the experimental results for $(x - x_b)/h_b = 16.709$, $h/h_b = 0.563$. Local wave height is 6.32 cm, wave set-up is 1.34 cm, mean water depth is 11.2 cm, and wave height to water depth ratio is 0.564. The rate of vertical diffusion is about 0.1–0.2$C$, and decreases slightly with depth. Comparing Fig. 6 to Fig. 7, it is seen that the fluid kinematics and the turbulence transport at these two stations have similar distributions, which suggests that some state of dynamical equilibrium is established in the inner surf zone. In the ideal situation where self-preservation exists, the structure of turbulence and the kinematic relations would remain similar at different stations if nondimensionalized with local length and velocity scales. In addition, the length and velocity scales will be functions of $x$ alone. Since the equations of motion permit self-preservation only in special cases, it is likely that turbulent flows in the inner surf zone are only approximately self-preserving, so that the scaling laws vary slowly in the $x$ direction. The normalized results presented in Figs. 6 and 7 indicate that the local water depth $h$ and the phase velocity $\sqrt{gh}$ relate to the length scale and velocity scale of turbulence in important way. This is to be expected since surf-zone turbulence originates from instabilities of waves therefore the dynamics of turbulence

should be related to the wave characteristics. However, the relation is probably far more complicated. For instance, it was found in a strong plunging breaker (Ting and Kirby, 1995) that $\sqrt{g(H+h)}$ provides a better estimate of the phase velocity and presumably the velocity scale, which suggests that the wave height is also an important length scale. To establish the scaling laws, it is necessary to investigate the structure of turbulence systematically for a wide range of wave conditions.

Our study indicates that there is a significant difference between spilling and plunging breakers also long after the breaking starts. It was shown in Ting and Kirby (1994) that turbulent kinetic energy is transported seaward by the mean flow under a spilling breaker and landward under a plunging breaker. This phenomenon is related to the time scales of wave motion and large-eddy motion, which are in turn related to the rate of energy transfer from wave to turbulence; for a detailed discussion of this aspect of surf-zone turbulence the interested reader is referred to Ting and Kirby (1994). It will be shown in this paper that the structures of turbulence in spilling and plunging breakers are indeed different. The simplest index of structure is the relative values of the components of the Reynolds stress tensor. In a two-dimensional surf zone the important Reynolds stresses are $\overline{u'^2}$, $\overline{w'^2}$ and $\overline{u'w'}$. Fig. 8 plots the vertical distributions of $\overline{w'^2}/\overline{u'^2}$ at different stations in the surf zone. Research in turbulent shear flows has shown that the relative values of the components of turbulent velocity fluctuations depend on the nature of turbulent flows and are similar for all flows of a single family. For example, the value of $\overline{w'^2}/\overline{u'^2}$ is 0.71 in plane jet, 0.77 in plane wake and 0.51 in the outer region of boundary layer (Townsend, 1976). Hence, the difference between the two groups of free turbulent flows is much less than that between the boundary-free shear flow and the wall-bounded shear

flow; this is related to the effect of the flow boundaries on the turbulent motion. The profile of $\overline{w'^2}/\overline{u'^2}$ is presented in Fig. 8a for the spilling breaker case. It is seen that the ratio $\overline{w'^2}/\overline{u'^2}$ varies considerably across the surf zone but its variation over depth is small everywhere. Velocity measurements and visual observations indicate that turbulent energy is generated in the crest region and spread downward by moderate-scale eddies. The descending eddies are subject to straining by a strong shear flow (see Fig. 7a). Indeed, in comparing the mean flows in spilling and plunging breakers (Ting and Kirby, 1994) it was found that horizontal velocities are virtually constant below trough level and above the bottom boundary layer in the plunging breaker, whereas large velocity gradients exist in the spilling breaker. Because of large strain rates (see Fig. 15) and slow spreading of turbulence in the spilling breaker, we should expect that pressure-velocity interactions will allow efficient energy transfer between velocity components thus maintain good ratio of $\overline{w'^2}/\overline{u'^2}$. For comparison, Fig. 8b plots the distribution of $\overline{w'^2}/\overline{u'^2}$ in a plunging breaker (Ting and Kirby, 1995); this result has not been presented before. It is seen that the value of $\overline{w'^2}/\overline{u'^2}$ decreases markedly with distance from the surface. This is because the variation of $\overline{u'^2}$ over depth is very small, whereas $\overline{w'^2}$ decreases rapidly downward. The latter suggests that the inhomogeneity of turbulence is caused by the presence of the solid bottom. In the plunging breaker, turbulent motion is dominated by large vortex-like eddies with large length and velocity scales. Because of this, turbulent diffusion is much faster. The large eddies quickly run into the bottom therefore vertical motion is restricted. In addition, we may expect that straining of large eddies should be less effective under the plunging breaker because the time scale of vertical mixing is much smaller than the characteristic time of the mean flow. These results indicate that the structural differences between spilling and

plunging breakers are related to the method of energy transfer from the organized wave-induced motion to the turbulent motion, and the effects of the mean flow and the solid boundary on the large eddies.

The determination of turbulent velocity correlations is the main problem in turbulence modeling. These correlations appear in the Reynolds stress tensor in the momentum equations and the triple-velocity tensor in the Reynolds-stress transport equations. Reynolds stresses have been studied by Stive and Wind (1982), Sakai et al. (1984), Nadaoka (1986) and Okayasu (1988), amongst others. Stive and Wind (1982) studied the depth and time-averaged momentum equations in a spilling breaker and found that the turbulent contribution to the radiation stress in the surf zone is weak. Sakai et al. (1984) studied the time variations of Reynolds stresses over one wave period in spilling and plunging breakers. They compared the magnitude of the terms in the $x$-momentum equation, and found that the Reynolds stress terms are small compared to the local acceleration and the convective terms. In Sakai et al. (1984), turbulent velocity fluctuations were obtained by filtering away the low frequencies from the measured signals. Since most of the turbulent energy is associated with the large-scale motions, it is likely that part of the turbulence has been omitted from their results. Okayasu et al. (1988) obtained the time-mean eddy viscosity from the time-mean Reynolds stress $\overline{u'w'}$ and the vertical gradient of undertow in spilling and plunging breakers. They found that Reynolds stress and eddy viscosity decrease with distance from the surface. It would be interesting to study the correlation coefficient between $u'$ and $w'$ in spilling versus plunging breakers. In most turbulent shear flows the value of $-\overline{u'w'}/(\overline{u'^2}\,\overline{w'^2})^{\frac{1}{2}}$ is about 0.4, and this value varies only little across any flow and also little from flow to flow. From physical reasoning we expect that the correlation between $u'$ and $w'$

should be better in spilling breakers due to more effective straining of eddies by the mean flow.

The velocities $u$ and $w$ were not measured simultaneously when we conducted the experiments at University of Delaware. A 1 on 35 sloped false bottom was later installed in the two-dimensional wave tank at Texas A&M University. This slope was built for an experimental study of surf-zone turbulence in irregular waves (Sultan and Ting, 1993). In this tank we have repeated some experiments for the spilling breaker case. We measured $u$ and $w$ simultaneously in the inner surf zone using a two-component laser-Doppler anemometer. Typical examples of the temporal variations of the turbulent kinetic energy $k$ and the corresponding correlation coefficient between $u'$ and $w'$ are shown in Figs. 9a and 9b. The value of $\widetilde{u'w'}/(\widetilde{u'^2}\widetilde{w'^2})^{\frac{1}{2}}$ varies between 0 and -0.5. The correlation coefficient is around -0.4 at the turbulent front and decreases as the turbulence decays. Considering that the Reynolds stress terms are most important during period of high turbulence intensity, these results provide some support for the use of a correlation coefficient of -0.4 between $u'$ and $w'$ in the spilling breaker case. Fig. 9c plots the variation of $\overline{u'w'}/(\overline{u'^2}\,\overline{w'^2})^{\frac{1}{2}}$ with depth. The correlation coefficient varies between -0.1 and -0.3 with the best correlation between $u'$ and $w'$ found at some distance below the trough level.

Fig. 10 plots the temporal variations of the correlation coefficient between $u'^2$ and $u'$ in the inner surf zone; similar results are found in the outer surf zone. This correlation represents the transport of turbulent kinetic energy by the horizontal component of turbulent velocity fluctuations. It is seen that the correlation coefficient is mostly positive, and its temporal variation over a wave period is similar to that of the turbulent velocity fluctuations (Figs. 7c and 7d). Good correlation between $u'^2$ and $u'$ is found where turbulence intensity is high;

the correlation coefficient there is between 0.3 and 0.5. Also, the correlation is generally better at some distance below the trough level. The results are consistent with slow spreading of turbulence from the surface by moderate-scale eddies. As the eddies evolve vortex stretching tends to maintain good correlation between $u'^2$ and $u'$. The temporal variations of the correlation coefficient between $w'^2$ and $w'$ are plotted in Fig. 11. The results are similar except that the correlation coefficient is mostly negative which means that turbulent energy is transported downward by turbulent velocity fluctuations.

Velocity spectra in a laboratory surf zone have been studied by Hattori and Aono (1985). In that study, wave breaking was initiated at the edge of a horizontal shelf by a 1 on 20 slope in front. They found that the slopes of the velocity spectra at high frequencies were approximately -3, whereas fully developed turbulent flows should have a slope of -5/3. This discrepancy may be a consequence of their experimental arrangement, that the shelf has hindered the wave breaking process thus turbulence cannot attain a fully developed state. Similar situation was observed in the outer surf zone in this present study. It can be shown that the structure of turbulence in a laboratory surf zone is independent of viscosity. Therefore, Froude scaling should apply for the large-scale turbulent motion as well as the wave motion. In addition, viscous transport of turbulent energy can be neglected. Fig. 12 plots the velocity spectra of wave and turbulence, and of turbulence alone for $(x - x_b)/h_b = 16.709$. The velocity spectra are presented for $(z-\overline{\zeta})/h = -0.3875$ (Figs. 12a and 12b) and $(z-\overline{\zeta})/h = -0.8339$ (Figs 12c and 12d); trough level is located at $(z - \overline{\zeta})/h \approx -0.25$. Fig. 12 shows that most of the turbulent energy is associated with the large-scale motions in the wave frequency range. The slopes of the velocity spectra at high frequencies are closely approximated by a -5/3 slope, corresponding to that

for the inertial subrange. This implies that the turbulent Reynolds number is very large. The turbulent Reynolds number is defined as $Ul/\nu$. The magnitude of turbulent Reynolds number necessary for an inertial subrange to exist is of the order of $10^5$ (Tennekes and Lumley, 1972). At high Reynolds numbers there is a large difference in the sizes of the large eddies of turbulence production and the small eddies of energy dissipation so that the large-scale structure of turbulence is independent of fluid viscosity. Furthermore, it may be observed that the velocity spectra of the horizontal and vertical components coincide at frequencies higher than 2 Hz. This local isotropy does not exist if the Reynolds number is not large enough. This is because the large eddies have preferred directions due to the strain rate of the mean flow, and eddies of smaller size are subject to the strain rate of large eddies. However, if the Reynolds number is very high there is little direct interaction between small eddies and large eddies so that the small-scale structure of turbulence is very nearly isotropic.

*3.2. Turbulence transport equation*

Eq. 5 is analyzed to determine the relative importance of the individual turbulence transport terms. The local time rate of change of turbulent kinetic energy $\partial k/\partial t$, and the convection terms $\partial \tilde{u}k/\partial x$ and $\partial \tilde{w}k/\partial z$ are found from the phase-averaged velocities. The pressure fluctuations and the fluctuating rate of strain cannot be measured. Therefore, turbulence transport by pressure fluctuations is not studied; dissipation is studied based on the classical relation given by Eq. 12. Transport of turbulent energy by turbulent velocity fluctuations is given by $\partial \widetilde{u'k'}/\partial x$ in the horizontal direction and $\partial \widetilde{w'k'}/\partial z$ in the vertical direction. We have measured the components $\frac{1}{2}\partial \widetilde{u'^3}/\partial x$ and $\frac{1}{2}\partial \widetilde{w'^3}/\partial z$ only. These experimental data, although incomplete, can still provide important insights

into the nature of turbulent diffusion. We have to assume that the correlation coefficient between $u'$ and $w'$ is equal to 0.4 in order to estimate turbulence production. For example, the major production term $\widetilde{u'w'}\partial\tilde{u}/\partial z$ is estimated by $0.4(\widetilde{u'^2}\widetilde{w'^2})^{\frac{1}{2}}\partial\tilde{u}/\partial z$. The other production terms are found in a similar manner. On the basis of Fig. 9b we expect that the error associated with this estimation will not exceed $\pm 20\%$ in the production phase. The error will be larger in the decay phase but turbulence production there is small anyway. Partial derivatives in $z$ and $t$ are calculated using central finite difference method. We have used the transformation $\partial/\partial x = -C^{-1}\partial/\partial t$ to calculate the partial derivatives in $x$. This assumes that the wave is of permanent form, which is substantially accurate since the time scale of change in the wave shape is much larger than the sampling time interval of 0.01 s. Finally, the spatial and temporal derivatives are low-pass filtered at 10 Hz to reduce measurement noise.

Some typical results are presented in Figs. 13–14. In these figures, the solid line is $\partial k/\partial t$, the dashed line is $-(\partial\tilde{u}k/\partial x + \partial\tilde{w}k/\partial z)$, the dotted line is $-\frac{1}{2}\partial\widetilde{u'^3}/\partial x$, and the dashdot line is $-\frac{1}{2}\partial\widetilde{w'^3}/\partial z$. The turbulence transport terms are nondimensionalized by $C^2T^{-1}$, where T is the wave period. The results for $(x-x_b)/h_b = 4.397$ are plotted in Figs. 13a and 13b for $(z-\overline{\zeta})/h = -0.3194$ and $(z-\overline{\zeta})/h = -0.7194$, respectively; trough level is located at $(z-\overline{\zeta})/h \approx -0.2$. We believe that the large fluctuations in $\partial k/\partial t$ around $t/T = 0.2$ in Fig. 13a is produced by convection of turbulence structure past the probe as turbulent energy spreads downward. Large eddies are formed around the wave front; these eddies produce bursts of turbulence as they are convected past the probe. The procedure of phase averaging smooths out the fluctuation of $\partial k/\partial t$ caused by the passage of eddies but will not remove the fluctuation entirely. This is because the eddies in successive breakers are not completely random in space and time.

We observed that the fluctuation of $\partial k/\partial t$ is more pronounced in the plunging breaker case (see Ting and Kirby, 1995) than in the spilling breaker, which suggests that large-scale eddy motions are more organized in strong breakers.

The measured data show that turbulent energy is removed by the upward current under the wave front; the energy removed is replaced by horizontal advection and turbulent diffusion. It is found that the term $-\frac{1}{2}\partial\widetilde{u'^3}/\partial x$ is vanishingly small everywhere. This term is the major part of $-\partial\widetilde{u'k'}/\partial x$, which represents the gradient transport of $k$ by the horizontal component of turbulent velocity fluctuations. On the contrary the term $-\frac{1}{2}\partial\widetilde{w'^3}/\partial z$, which is part of $-\partial\widetilde{w'k'}/\partial z$, is much larger, reflecting the importance of vertical diffusion. The results for $(z-\overline{\zeta})/h = -0.7194$ are plotted in Fig. 13b. It is seen that the fluctuation of $\partial k/\partial t$ has decreased and the advection term has become small. Visual observations indicate that the vortex-like eddies degenerate into small-scale turbulence as they convect downward. This process destroys the organized nature of large-eddy motions. Therefore, the fluctuation of $\partial k/\partial t$ can be found not only in the phase around the wave crest but is more uniform in time.

The results for $(x-x_b)/h_b = 16.709$ are presented in Figs 14a and 14b; trough level is located at $(z-\zeta)/h \approx -0.25$. These results are similar to those from the outer surf zone. It is seen that advection is important near the surface, and the temporal variation of $\partial k/\partial t$ shows increasing disorder with distance from the surface. It may be observed in Fig. 14a that $\partial k/\partial t$ is composed of a slow modulation in time, and quasi-periodic fluctuations. We believe that the slow variation in $\partial k/\partial t$ is associated with the main turbulent motion which contains most of the turbulent kinetic energy, while the large fluctuations are caused by convection of large eddies past the probe. Townsend (1976) describes the main turbulent motion as structures which are larger than the small eddies

of local isotropy but small compared with the scale of inhomogeneity of the flow. Hence, the main turbulent motion is transported by the mean flow and the large eddies. In breaking waves, the large eddies are formed by the folding of the free surface, and have sizes comparable with the local wave height. Nadaoka et al. (1989) observed that the large eddies are initially two-dimensional, but break down into three-dimensional vortices descending obliquely downward. It is conjectured that the large eddies become unstable and degenerate into moderate-scale structure of the main turbulent motion. The quasi-periodicity in $\partial k/\partial t$ indicates that these large eddies are generated at regular interval and the process occurs repeatedly in an orderly fashion in successive breakers.

Our experiments suggest that the temporal variation of turbulent energy and its vertical distribution are determined primarily by turbulent diffusion. On the other hand, advection is only of second order importance, except near the surface. Therefore, it is important to correctly model the diffusion terms in order to appropriately predict the distribution of turbulent energy in spilling breakers. This conclusion is based on data obtained below trough level and well away from the bed.

The determination of the diffusion coefficient in the $k$-equation remains a difficult problem. Using Eq. 8 and the measured rate of vertical advance of turbulent front we estimate that $D$ is of order $0.1h\sqrt{gh}$. As discussed earlier this result is for "fully mixed" condition. The actual value of $D$ will likely be much smaller than this. Based on comparisons of computed and measured undertow velocity profiles Svendsen et al. (1987) estimated that the eddy viscosity $\nu_t$ is in the range $0.01$–$0.02h\sqrt{gh}$. These results put the Schmidt number $\sigma_t = \nu_t/D$ in the range 0.1–1.0. For comparison, $\sigma_t$ is about 0.9 in near-wall flows, and 0.5 in plane jets and mixing layers (Rodi, 1984). It is not clear whether a constant

value of $D$ can be used below trough level. We expect that vortex stretching reduces the eddy size with distance from the surface, while dissipation destroys the small eddies and thus effectively increases the eddy size and the mixing length. The importance of transport of length scale may be seen by comparing the time scale of turbulent diffusion with the characteristic time of straining and the dissipation time scale. From the vertical advance of turbulent front the time scale of mixing is estimated to be of the order of one wave period. The characteristic time of straining is inversely proportional to the strain rate of the mean flow. As an example, Fig. 15 plots the temporal variation of the strain rate $\gamma_{xz} = \partial\tilde{u}/\partial z + \partial\tilde{w}/\partial x$ for different elevations at $(x - x_b)/h_b = 16.709$. Comparing Fig. 15 with Fig. 7, it is seen that high turbulence intensity is associated with high strain rate, thus turbulent diffusion and vortex stretching are related. It can be concluded from Fig. 15 that the characteristic time of straining is much shorter than the wave period of 2.0 s, therefore effect of vortex stretching is important. The decay time of the large eddies is proportional to $l/U$, where $U$ and $l$ should be of the order of the r.m.s. turbulent velocity and the local wave height, respectively. Taking $U \approx 0.05C$ from Fig. 7c, and $l \approx H = 0.56h$, the turbulence decay time is between 1 to 2 s thus effect of dissipation is also important. This analysis indicates that transport processes could be important in the determination of length scale in a spilling breaker.

The major terms of turbulence production are presented in Fig. 16 for the outer surf zone and Fig. 17 for the inner surf zone. The production terms are relatively small in the outer surf zone. The term $\widetilde{u'w'}\partial\tilde{u}/\partial z$ (dashed line) represents energy removed from the mean flow by the work of Reynolds shear stress against the mean velocity gradient $\partial\tilde{u}/\partial z$. In many shear flows this term accounts for most of the turbulence production whereas the term $\widetilde{u'w'}\partial\tilde{w}/\partial x$ is

considerably smaller. The production term caused by normal-stress difference $-(\widetilde{u'^2} - \widetilde{w'^2})\partial\tilde{u}/\partial x$ is generally small since it is the difference between $\widetilde{u'^2}$ and $\widetilde{w'^2}$ that determines the contribution to turbulence production. In the outer surf zone all the production terms are small and it is not clear which term dominates.

The production terms are considerably larger in the inner surf zone (Fig. 17). The term $\widetilde{u'w'}\partial\tilde{u}/\partial z$ is the only major production term; the relative contributions of the other terms are small. It is interesting to see that the value of $\widetilde{u'w'}\partial\tilde{u}/\partial z$ is quite large, but this has no effect on $\partial k/\partial t$. This suggests that the dissipation rate is also high so that production is roughly balanced by dissipation. In most shear flows production and dissipation are of the same order of magnitude even if they do not balance. Similar results are found at other elevations. It is found that although turbulence production below trough level amounts to only a small portion of wave energy loss, the leading production term is of the same order of magnitude as the major transport terms. Hence, we cannot neglect turbulence production below trough level since this would exaggerate the effect of dissipation. It must be realized that it is the difference between production and dissipation that contributes to the rate of change of turbulent kinetic energy.

We did not measure the dissipation rate because the fluctuating rate of strain $s_{ij}$ cannot be measured reliably. In pure shear flows where the only nonvanishing velocity component is $\tilde{u}$ in the $x$ direction, Taylor hypothesis may be used to compute the turbulent velocity gradient from the local time derivative, that is

$$\frac{\partial}{\partial t} = -\tilde{u}\frac{\partial}{\partial x} \tag{11}$$

provided that $\tilde{u} \gg u'$. This condition is not satisfied in surf-zone turbulence since the turbulent velocity fluctuations created by the large eddies are not small

compared to the organized wave-induced velocities. The small eddies of energy dissipation are transported by the mean flow and the large eddies. Furthermore, turbulence is spread downward by obliquely descending vortices thus convective transport of small-scale turbulence is substantially three-dimensional under a spilling breaker. Because of this, it would be very difficult to determine the convection velocity unambiguously for this wave condition. Svendsen (1987a) modeled the dissipation rate $\epsilon$ through the classical relation

$$\epsilon = -\frac{C_D}{l} k^{\frac{3}{2}} \tag{12}$$

where $C_D \approx 0.09$ is an empirical constant (see, Launder and Spalding 1972). For the length scale he used $l = 0.2h$ for the spilling breaker case in Stive and Wind (1982). Svendsen (1987a) then computed the wave energy loss from the wave decay and assumed that all this loss was converted into turbulent energy. In this way, he estimated that only 2–5% of the total turbulent energy production is dissipated below trough level.

It would be interesting to estimate the turbulence production below trough level and compare it with the wave energy loss. The production rate averaged over one wave period is plotted in Fig. 18 for different stations in the surf zone. Turbulence production is estimated by $0.4(\widetilde{u'^2}\widetilde{w'^2})^{\frac{1}{2}}\partial\tilde{u}/\partial z$ since $\widetilde{u'w'}\partial\tilde{u}/\partial z$ is the only major production term in the inner surf zone. It is seen that the production rate decreases with distance from the surface, but the variation over depth is small. In the inner surf zone, the production rate remains similar at different stations. Turbulent energy production below trough level is found from Fig. 18 by numerically integrating the production rate from the bottom to the trough level, i.e.

$$Production = \frac{0.4}{hT} \int_{-d}^{\zeta_t} \int_0^T \frac{(\widetilde{u'^2}\widetilde{w'^2})^{\frac{1}{2}}\partial\tilde{u}/\partial z}{(C^2/T)} dt dz \tag{13}$$

where $z = \zeta_t$ is the trough level. It is found that in the inner surf zone 3–6% of the total turbulent energy production occurs below trough level. The production is likely overestimated because of using a constant correlation coefficient of 0.4. The dissipation is also estimated using Eq. 12 with $l = 0.1h$. The results are plotted in Fig. 19. Comparing Fig. 19 with Fig. 18, the dissipation rate is larger than the production rate, which should be the case since there is diffusion of turbulent energy down through the trough level. The total energy dissipation below trough level is 7–10% of the wave energy loss. If we use $l = 0.2h$ the dissipation rate will be similar to the value found by Svendsen (1987a). However, the dissipation rate would be smaller than the production rate which is in contradiction with the finding that surface-generated turbulence is convected downward and dissipated below trough level. This result suggests that the mixing length should be somewhat less than $0.2h$ for the spilling breaker case.

## 4. Conclusions

The structure of turbulence in a spilling breaker has been studied experimentally. The study has focused on the region below trough level and above the bottom boundary layer. The area studied covers the outer surf zone through the inner surf zone. The objective of the study is to understand the individual turbulence transport processes to provide a scientific basis for modeling surf-zone turbulence. The following main conclusions can be drawn from this investigation:

1. Turbulence structure in a spilling breaker is tied in a direct way to the breaking wave characteristics. It is suggested that the length and velocity scales of the large eddies are determined by the rate of energy transfer from the organized wave-induced motion to the turbulent motion, and the size of

the surface roller. Spilling breakers differ from plunigng breakers primarily in the way in which energy is supplied to the turbulence, and the effects of the mean flow and the solid bottom on the large-scale turbulence. It can be shown that the important parameters are the wave period, the length and velocity scales of the large eddies, and the local water depth. These parameters govern the way in which turbulent energy is transported by mean flow and turbulent fluctuations, and thus the temporal and spatial variations of turbulence intensity.

2. The surface roller is confined to a region near the crest of the wave in a spilling breaker. The size of the largest eddies is small compared to the local water depth and the r.m.s. turbulent velocity is small compared to the local wave celerity. The time scales of vertical diffusion and energy dissipation are comparable to the wave period. Surface-generated turbulence is spread slowly downward by turbulent diffusion. The temporal variation of turbulent kinetic energy at a fixed point is related to the vertical advance of the turbulent front.

3. The mixing length is estimated from the measured rates of vertical advance of turbulent front. The mixing length is also found by balancing production and dissipation below trough level. The results are consistent with the findings in previous studies. It is suggested that $l$ is in the range 0.1–0.2$h$.

4. The structure of turbulence and the kinematic relations remain similar at different stations in the inner surf zone. Transformation of wave and turbulence characteristics across the surf zone is gradual.

5. The correlation coefficient between $u'$ and $w'$ varies during one wave cycle. A correlation coefficient of about -0.4 is found where the turbulence intensity

is high. The best correlation between $u'$ and $w'$ is found at some distance below the trough level.

6. Turbulent flow is well developed in the inner surf zone. The velocity spectra reveals an inertial subrange with -5/3 slope. Most of the turbulent energy is in the wave frequency range. The structure of turbulence is virtually independent of fluid viscosity.

7. Transport of turbulent energy by mean flow is important mainly near the surface. The local time rate of change of turbulent kinetic energy does not correlate well with either advection or production. This suggests that diffusion plays the most important role in turbulence transport. It is shown that vortex stretching and dissipation can change the size of the large eddies, thus the distributions of length scale may not be specified without solving the transport equation.

8. Turbulence production below trough level amounts to only a small portion of the wave energy loss. However, the major production term is of the same order of magnitude as the local time rate of change of turbulent kinetic energy, thus production cannot be neglected. The fact that $\partial k/\partial t$ and turbulence production are poorly correlated suggests that production is roughly balanced by energy dissipation, since it is their difference which contributes to the rate of change of turbulent energy.

**Acknowledgements**

This study was funded by the Office of Naval Research under contract N-00014-90-J168. F.C.K.T also acknowledges the support of the Texas Higher Education Coordinating Board through Grant 999903-261.

## References


Deigaard, R., Fredsœ, J. and Hedegaard, I. B., 1986. Suspended sediment in the surf zone. J. Waterw. Port Coastal Ocean Eng. ASCE, 112: 115–128.

Deigaard, R., Fredsœ, J. and Hedegaard, I. B., 1987. (Closure of) suspended sediment in the surf zone. J. Waterw. Port Coastal Ocean Eng. ASCE, 113: 557–562.

Deigaard, R., Justesen, P. and Fredsœ, J., 1991. Modelling of undertow by a one-equation turbulence model. Coastal Eng., 15: 431–458.

Hattori, M. and Aono, T., 1985. Experimental study on turbulence structures under breaking waves. Coastal Eng. in Japan, 28: 97–116.

Launder, B. E. and Spalding, D. B., 1972. Mathematical models of turbulence. Academic Press.

Mizuguchi, M., 1986. Experimental study on kinematics and dynamics of wave breaking. In: Proc. 20th Int. Coastal Eng. Conf., Taipei. ASCE, pp. 589–603.

Nadaoka, K., 1986. A fundamental study on shoaling and velocity field structure of water waves in the nearshore zone. Tech. Report. No. 36, Dept. Civ. Eng., Tokyo Inst. Tech., Japan, 125pp.

Nadaoka, K. and Kondoh, T., 1982. Laboratory measurements of velocity field structure in the surf zone by LDV. Coastal Eng. in Japan, 25: 125–146.

Nadaoka, K., Hino, M. and Koyano, Y., 1989. Structure of the turbulent

flow field under breaking waves in the surf zone. J. Fluid Mech., 204: 359–387.

Okayasu, A., Shibayama, T. and Nimura, N., 1986. Velocity field under plunging waves. In: Proc. 20th Int. Coastal Eng. Conf., Taipei. ASCE, pp. 660–674.

Okayasu, A., Shibayama, T. and Horikawa, K., 1988. Vertical variation of undertow in the surf zone. In: Proc. 21th Int. Coastal Eng. Conf., Malaga. ASCE, pp. 478–491.

Peregrine, D. H. and Svendsen, I. A., 1978. Spilling breakers, bores and hydraulic jumps. In: Proc. 16th Int. Coastal Eng. Conf., Hamburg. ASCE, pp. 540–550.

Rodi, W., 1984. Turbulence models and their application in hydraulics—A state of the art review. IAHR, 104 pp.

Sakai, T., Inada, Y. and Sandanbata, I., 1982. Turbulence generated by wave breaking on beach. In: Proc. 18th Int. Coastal Eng. Conf., Cape Town. ASCE, pp. 3–21.

Sakai, T., Sandanbata, I. and Uchida, M. 1984. Reynolds stress in surfzone. In: Proc. 19th Int. Coastal Eng. Conf., Houston. ASCE, pp. 42–53.

Stive, M. J. F., 1980. Velocity and pressure field of spilling breakers. In: Proc. 17th Int. Coastal Eng. Conf., Sydney. ASCE, pp. 547–566.

Stive, M. J. F. and Wind, H. J., 1982. A study of radiation stress and set-up in the surf zone. Coastal Eng., 6: 1–25.

Sultan, N. J. and Ting, F. C. K., 1993. Experimental study of undertow and turbulence intensity under irregular waves in the surf zone. In: Proc. 2nd Symp. Ocean Wave Measurement and Analysis, New Orlean. ASCE, pp. 602–613.

Svendsen, I. A., 1987a. Analysis of surf zone turbulence. J. Geophys. Res., 92(C5): 5115–5124.

Svendsen, I. A., 1987b. (Discussion of) suspended sediment in the surf zone. J. Waterw. Port Coastal Ocean Eng. ASCE, 113: 555–557.

Svendsen, I. A., Madsen, P. A. and Buhr Hansen, J., 1978. Wave characteristics in the surf zone. In: Proc. 16th Int. Coastal Eng. Conf., Hamburg. ASCE, pp. 520–539.

Svendsen, I. A., Schäffer, H. A. and Buhr Hansen, J., 1987. The interaction between the undertow and the boundary layer flow on a beach. J. Geophys. Res., 92(C11): 11845–11856.

Tada, Y., Sakai, T. and Obana, E., 1990. Variation of surf zone turbulence in a wave period. In: Proc. 22nd Int. Coastal Eng. Conf., Delft. ASCE, pp. 716–728.

Tennekes, H. and Lumley, J. L., 1972. A first course in turbulence. The MIT Press, 300 pp.

Ting, F. C. K. and Kirby, J. T., 1994. Observation of undertow and turbulence in a laboratory surf zone. Coastal Eng., 24: 51–80.

Ting, F. C. K. and Kirby, J. T., 1995. Dynamics of surf-zone turbulence in a

strong plunging breaker. Coastal Eng., 24: 177–204.

Townsend, A. A., 1976. The structure of turbulent shear flow. Cambridge University Press, 429 pp.

Wave conditions (the subscripts 0, $h$ and $b$ denote deep water, horizontal section and breaking point)

| $H_0$ (m) | $H_h$ (m) | $H_b$ (m) | $T$ (s) | $H_0/L_0$ | $x_b$ (m) | $d_b$ (m) |
|---|---|---|---|---|---|---|
| 0.127 | 0.125 | 0.163 | 2.0 | 0.020 | 6.400 | 0.196 |

Locations of measurements and water depths inside the surf zone

| $x$ (m) | 6.665 | 7.275 | 7.885 | 8.495 | 9.110 | 9.725 |
|---|---|---|---|---|---|---|
| $d$ (m) | 0.185 | 0.169 | 0.152 | 0.137 | 0.119 | 0.097 |
| $h$ (m) | 0.192 | 0.175 | 0.161 | 0.148 | 0.133 | 0.112 |

Table 1. Experimental conditions.

LIST OF FIGURES

$(z-\overline{\zeta})/h = -0.3875$; (c) and (d) $(z-\overline{\zeta})/h = -0.8339$. Solid lines are for instantaneous velocities. Dashed lines are for turbulent velocity fluctuations.

Fig. 13. Comparison of turbulence transport with local time rate of change of turbulent kinetic energy at $(x-x_b)/h_b = 4.397$, $h/h_b = 0.879$; $\partial k/\partial t$ (—), $-(\partial\tilde{u}k/\partial x + \partial\tilde{w}k/\partial z)$ (−−), $-\frac{1}{2}\partial\widetilde{u'^3}/\partial x$ $(\cdots)$, $-\frac{1}{2}\partial\widetilde{w'^3}/\partial z$ (−.). (a) $(z-\overline{\zeta})/h = -0.3194$, (b) $(z-\overline{\zeta})/h = -0.7194$.

Fig. 14. Comparison of turbulence transport with local time rate of change of turbulent kientic energy at $(x-x_b)/h_b = 16.709$, $h/h_b = 0.563$; $(\partial k)/\partial t$ (—), $-(\partial\tilde{u}k/\partial x + \partial\tilde{w}k/\partial z)$ (−−), $\frac{1}{2}\partial\widetilde{u'^3}/\partial x$ $(\cdots)$, $\frac{1}{2}\partial\widetilde{w'^3}/\partial z$ (−.). (a) $(z-\overline{\zeta})/h = -0.3875$. (b) $(z-\overline{\zeta})/h = -0.7446$.

Fig. 15. Phase-averaged strain rate $\gamma_{xz}$ at $(x-x_b)/h_b = 16.709$, $h/h_b = 0.563$. (a) $(z-\overline{\zeta})/h = -0.3875$, (b) $(z-\overline{\zeta})/h = -0.4768$, (c) $(z-\overline{\zeta})/h = -0.6554$, (d) $(z-\overline{\zeta})/h = -0.7446$.

Fig. 16. Comparison of turbulence production with local time rate of change of turbulent kinetic energy at $(x-x_b)/h_b = 4.397$, $(z-\overline{\zeta})/h = -0.3194$; $\partial k/\partial t$ (—), $0.4(\widetilde{u'^2}\widetilde{w'^2})^{\frac{1}{2}}\partial\tilde{u}/\partial z$ (−−), $0.4(\widetilde{u'^2}\widetilde{w'^2})^{\frac{1}{2}}\partial\tilde{w}/\partial x$ $(\cdots)$, $-(\widetilde{u'^2} - \widetilde{w'^2})\partial\tilde{u}/\partial x$ (−.).

Fig. 17. Comparison of turbulence production with local time rate of change of turbulent kinetic energy at $(x-x_b)/h_b = 16.709$, $(z-\overline{\zeta})/h = -0.3875$; $\partial k/\partial t$ (—), $0.4(\widetilde{u'^2}\widetilde{w'^2})^{\frac{1}{2}}\partial\tilde{u}/\partial z$ (−−), $0.4(\widetilde{u'^2}\widetilde{w'^2})^{\frac{1}{2}}\partial\tilde{w}/\partial z$ $(\cdots)$, $-(\widetilde{u'^2} - \widetilde{w'^2})\partial\tilde{u}/\partial x$ (−.).

Fig. 18. Variation of time-averaged production rate with depth; $h/h_b = 0.879$ (◯), 0.809 (▫), 0.744 (△), 0.668 (▽), 0.563 (•).

Fig. 19. Variation of time-averaged dissipation rate with depth; $h/h_b = 0.879$ (◯), 0.809 (▫), 0.744 (△), 0.668 (▽), 0.563 (•). Dissipation is normalized by $C^2/T$.

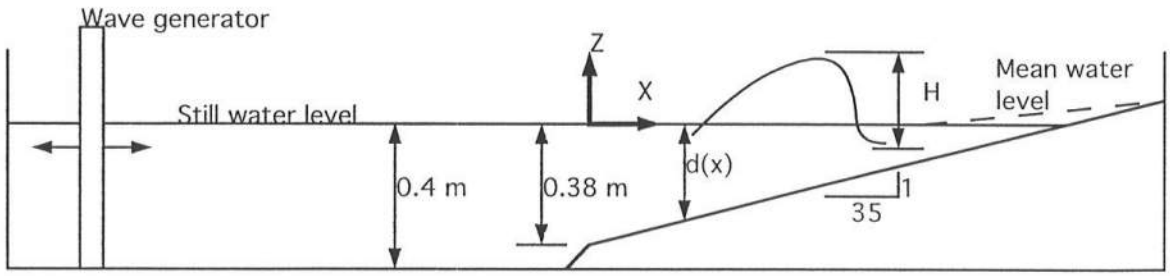
Wave generator
Z
X
H
Mean water level
Still water level
0.4 m
0.38 m
d(x)
1
35

FIGURE 1

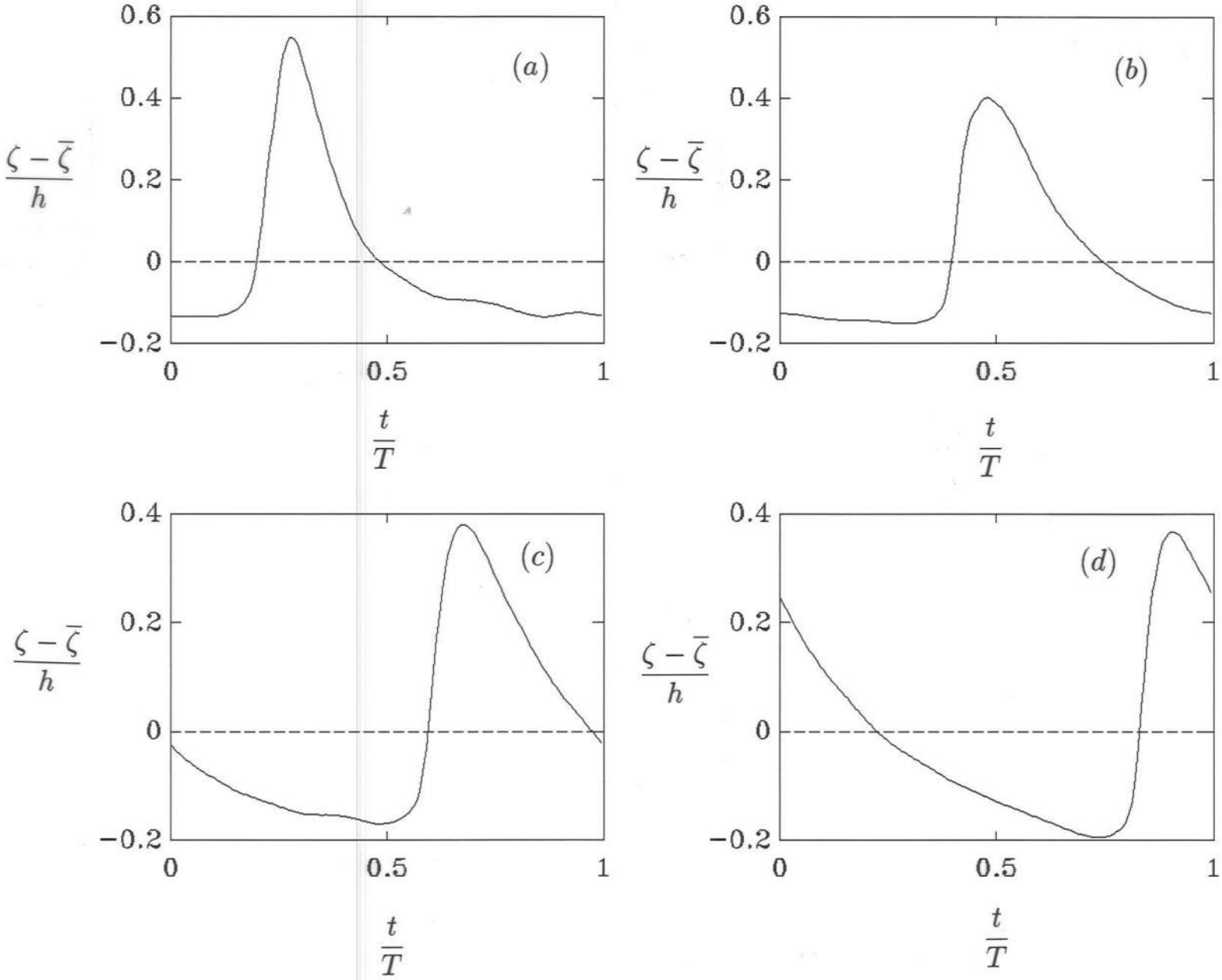


FIGURE 2

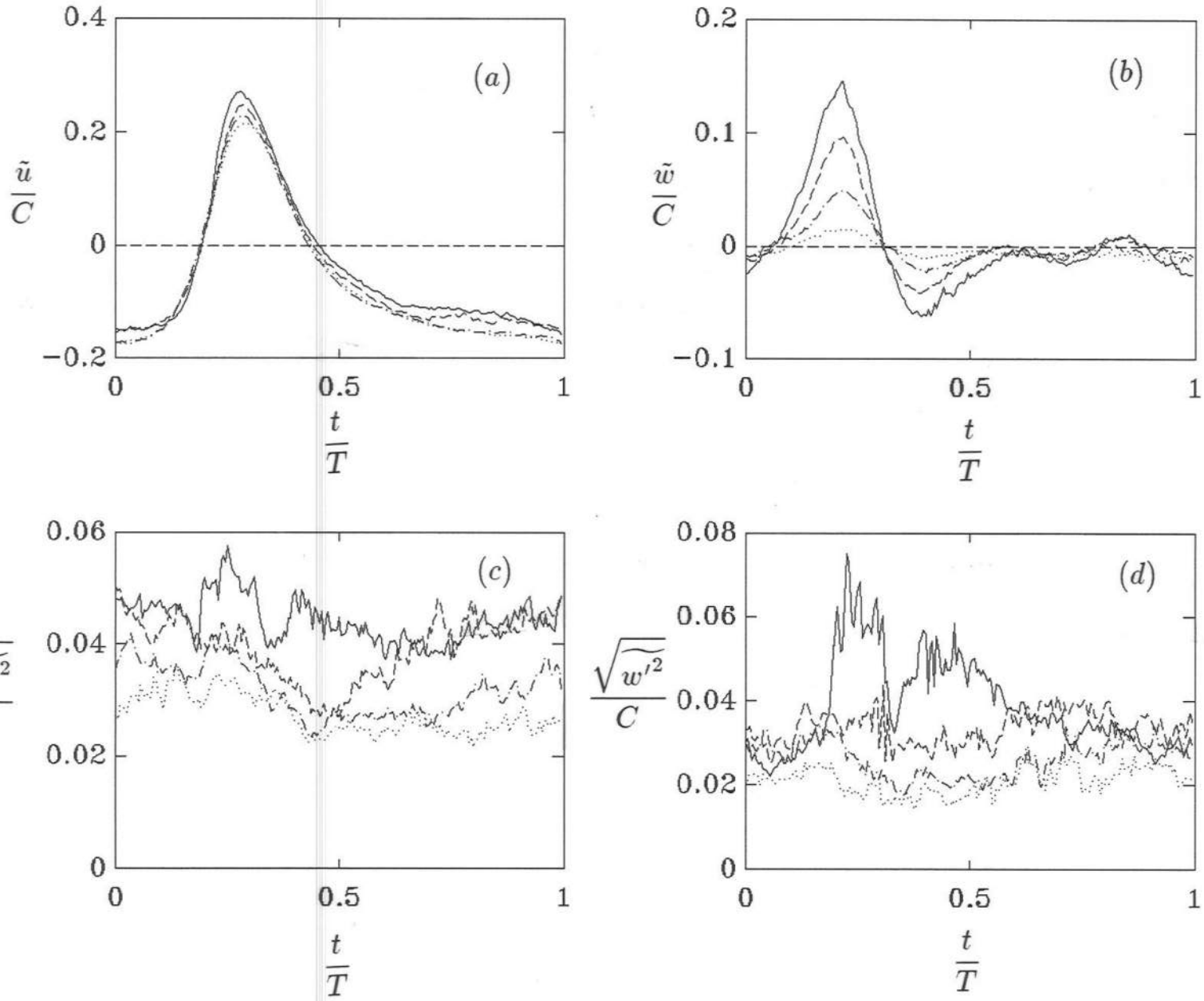
(a)
(b)
(c)
(d)
0.4
0.2
0
−0.2
0.2
0.1
0
−0.1
0.06
0.04
0.02
0
0.08
0.06
0.04
0.02
0
0.5
1
$\frac{\tilde{u}}{C}$
$\frac{\tilde{w}}{C}$
$\frac{\sqrt{\widetilde{u'^2}}}{C}$
$\frac{\sqrt{\widetilde{w'^2}}}{C}$
$\frac{t}{T}$

FIGURE 3

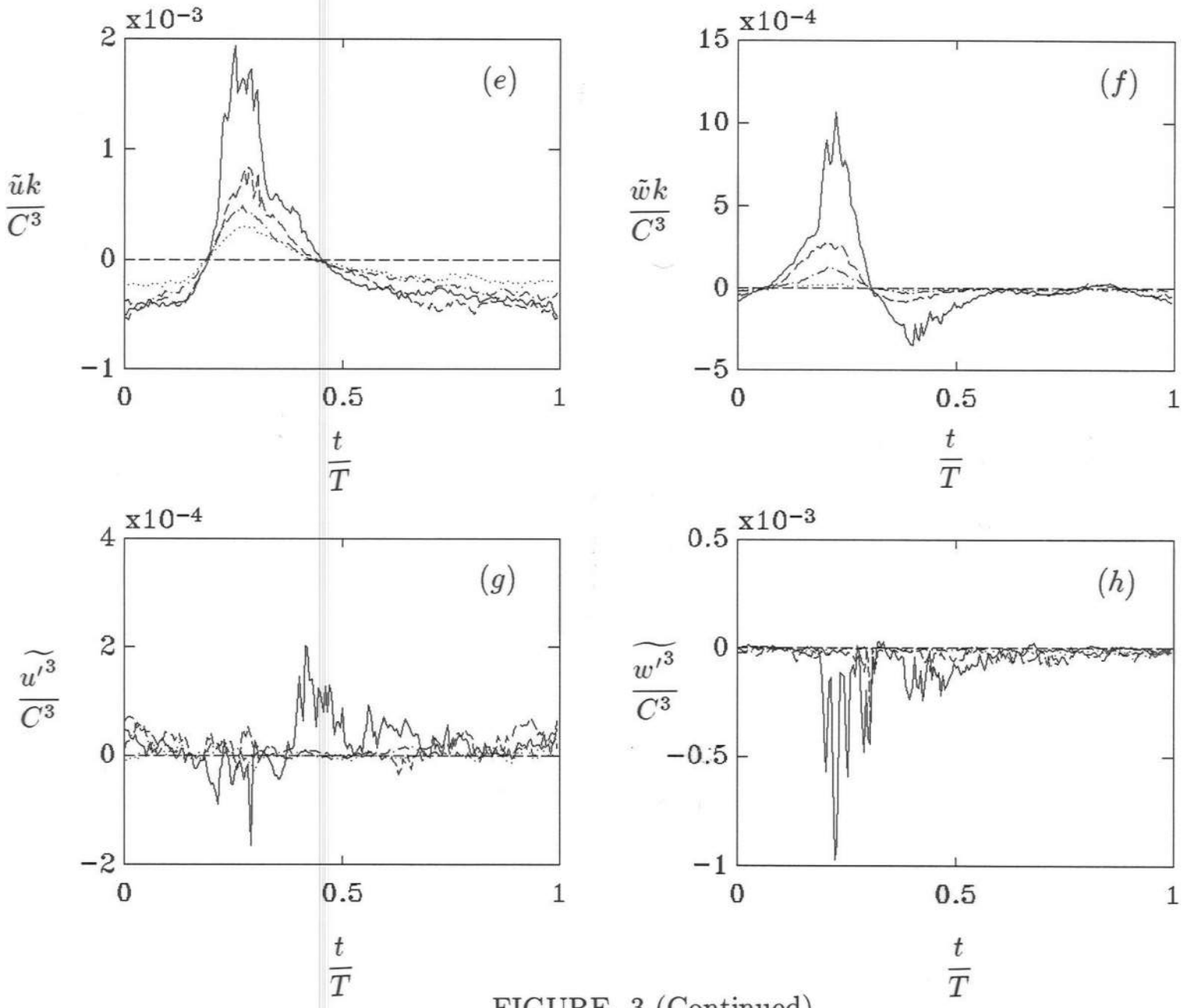


FIGURE 3 (Continued)

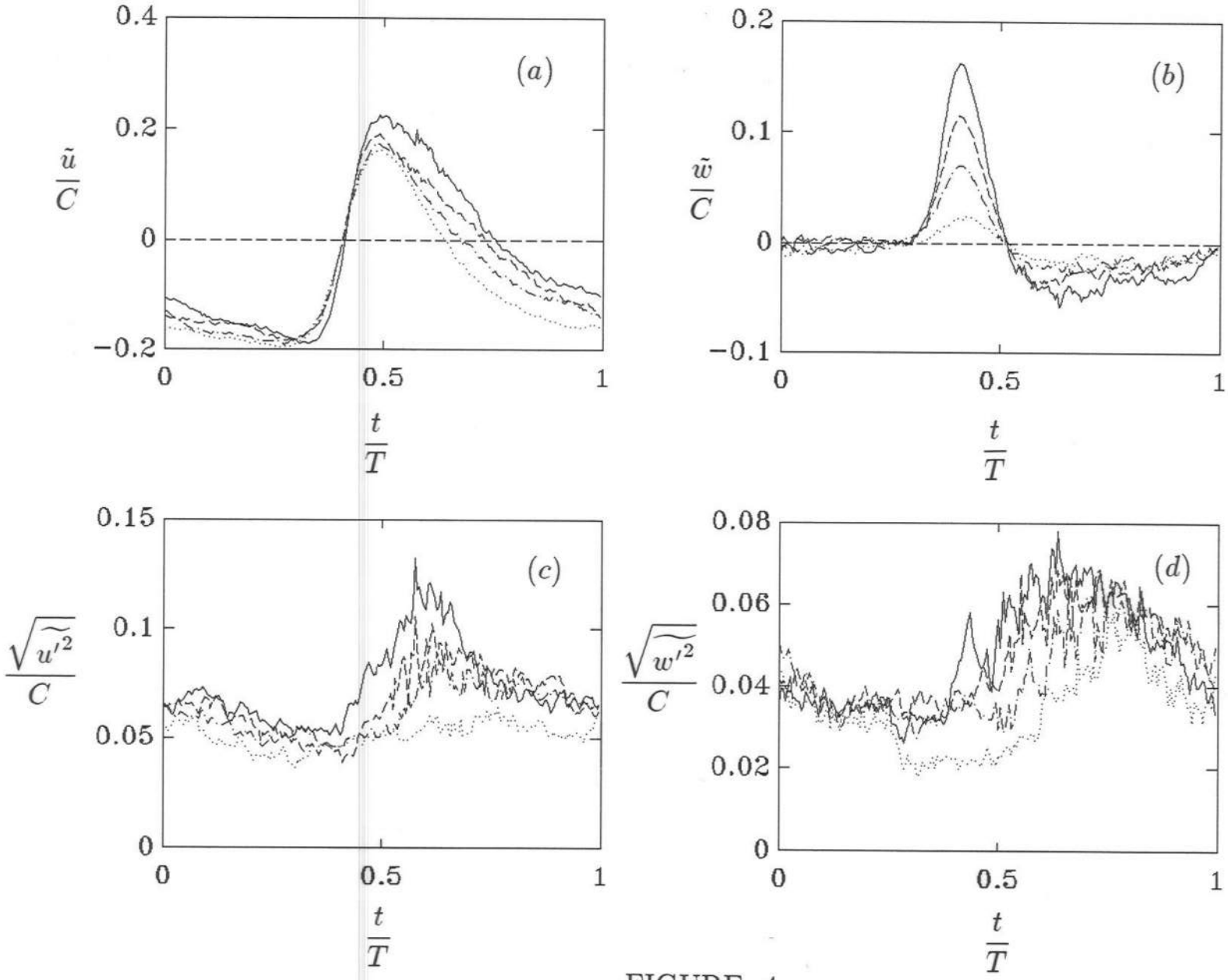
(a)
(b)
(c)
(d)
$\frac{\tilde{u}}{C}$
$\frac{\tilde{w}}{C}$
$\frac{\sqrt{\widetilde{u'^2}}}{C}$
$\frac{\sqrt{\widetilde{w'^2}}}{C}$
$\frac{t}{T}$
0.4
0.2
0
−0.2
0.1
−0.1
0.15
0.05
0.08
0.06
0.04
0.02
0
0.5
1

FIGURE 4

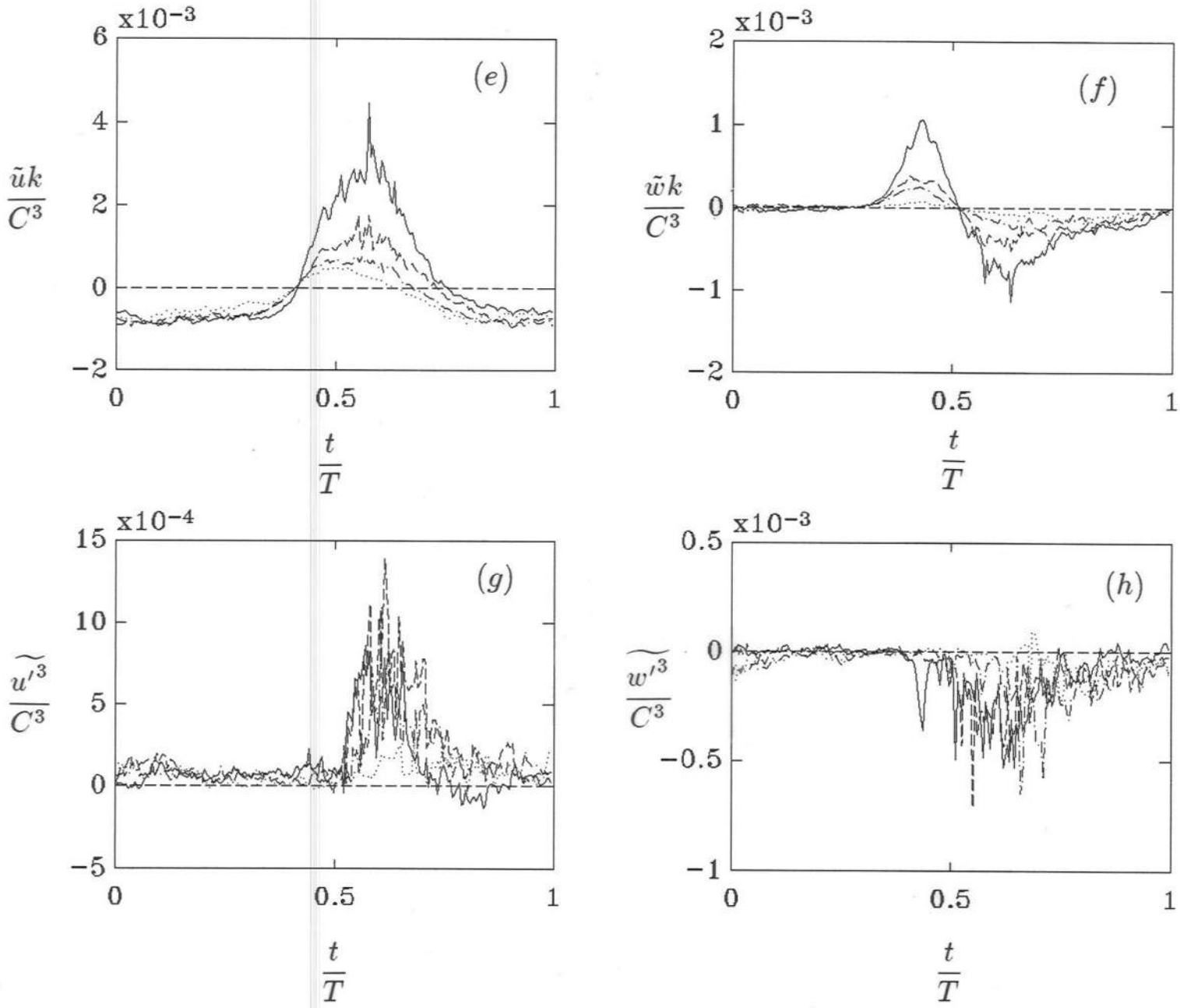


FIGURE 4 (Continued)

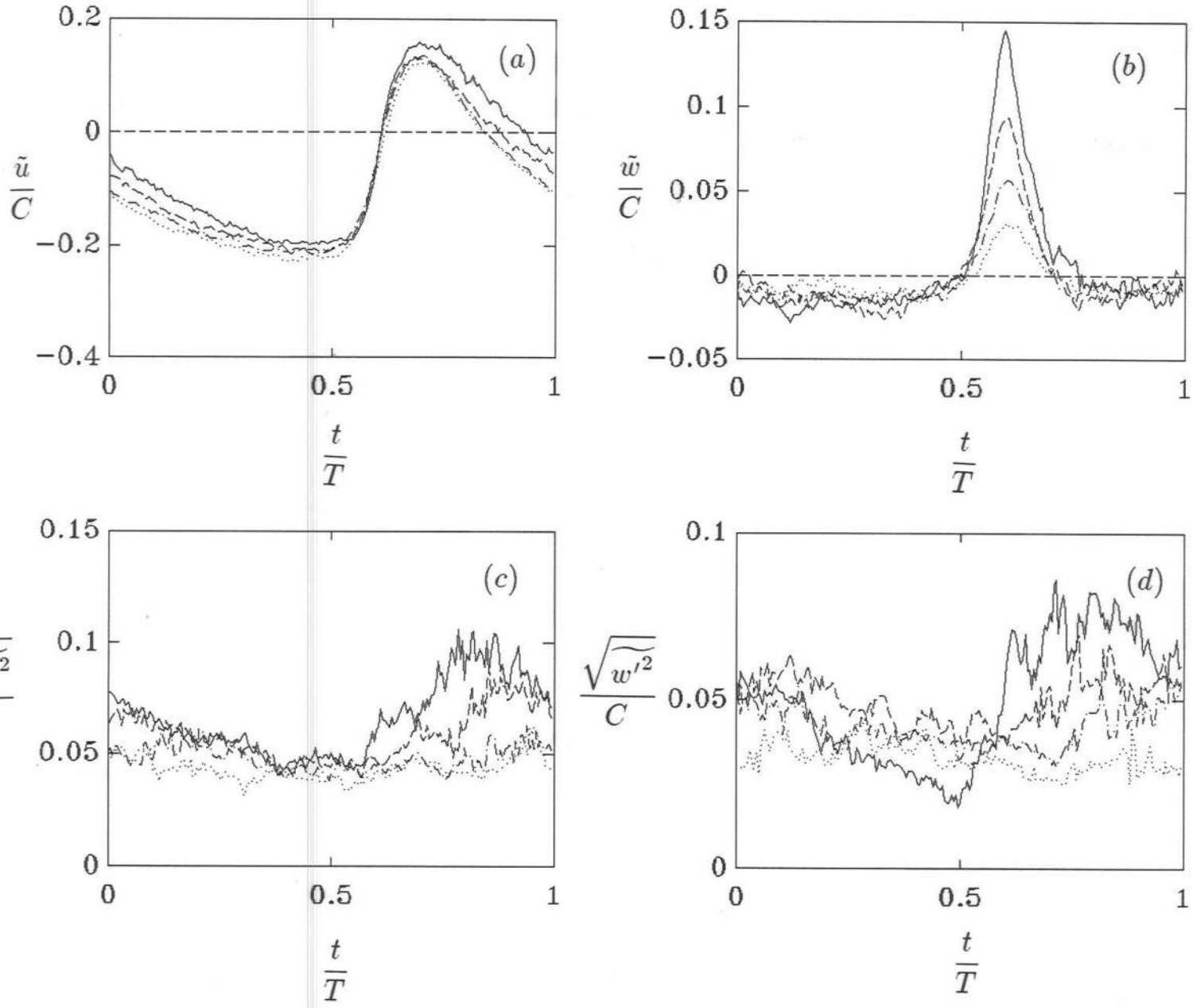
(a)
(b)
(c)
(d)
0.2
0
−0.2
−0.4
0.15
0.1
0.05
−0.05
0
0.5
1
$\frac{\tilde{u}}{C}$
$\frac{\tilde{w}}{C}$
$\frac{\sqrt{\widetilde{u'^2}}}{C}$
$\frac{\sqrt{\widetilde{w'^2}}}{C}$
$\frac{t}{T}$

FIGURE 5

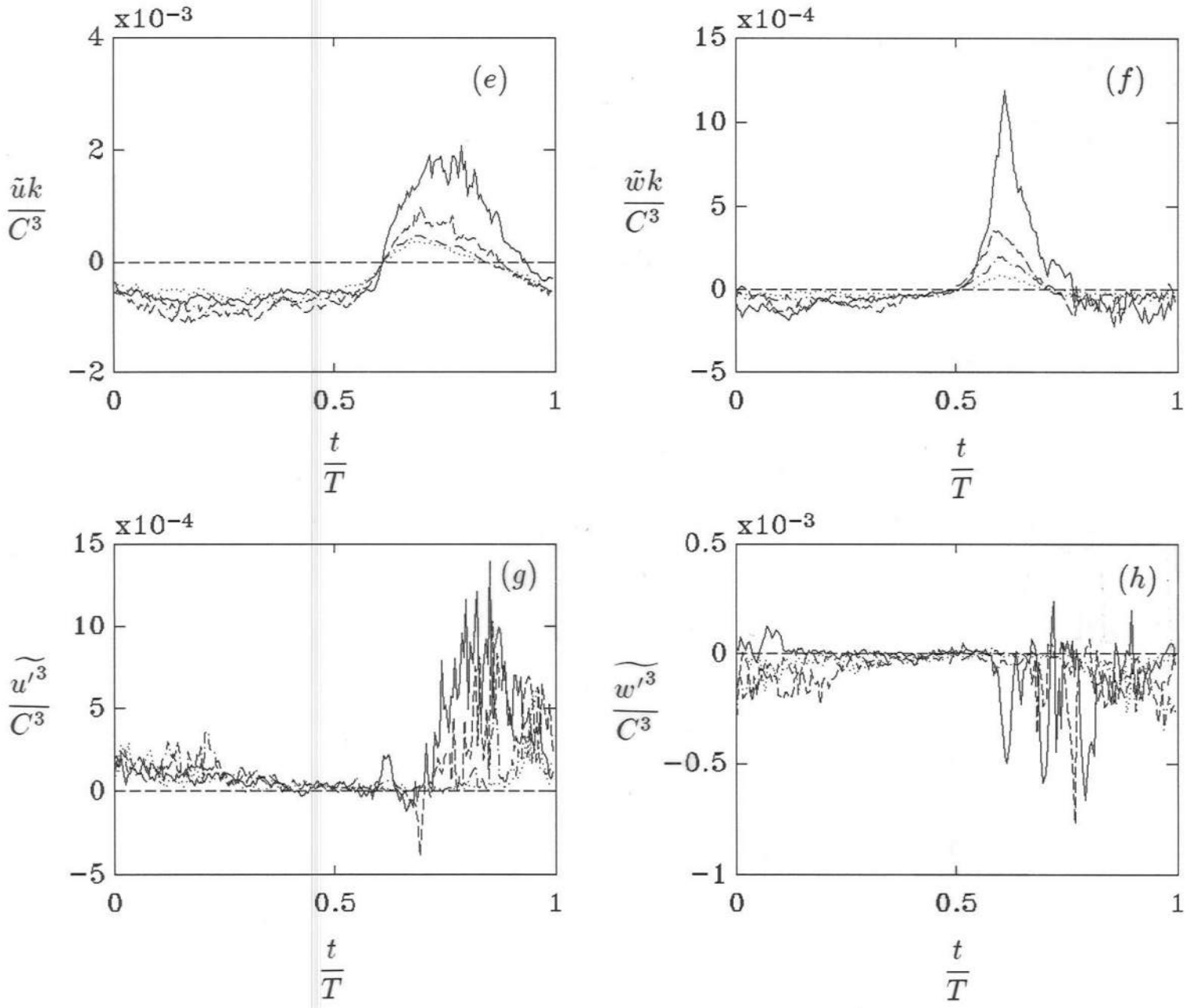


FIGURE 5 (Continued)

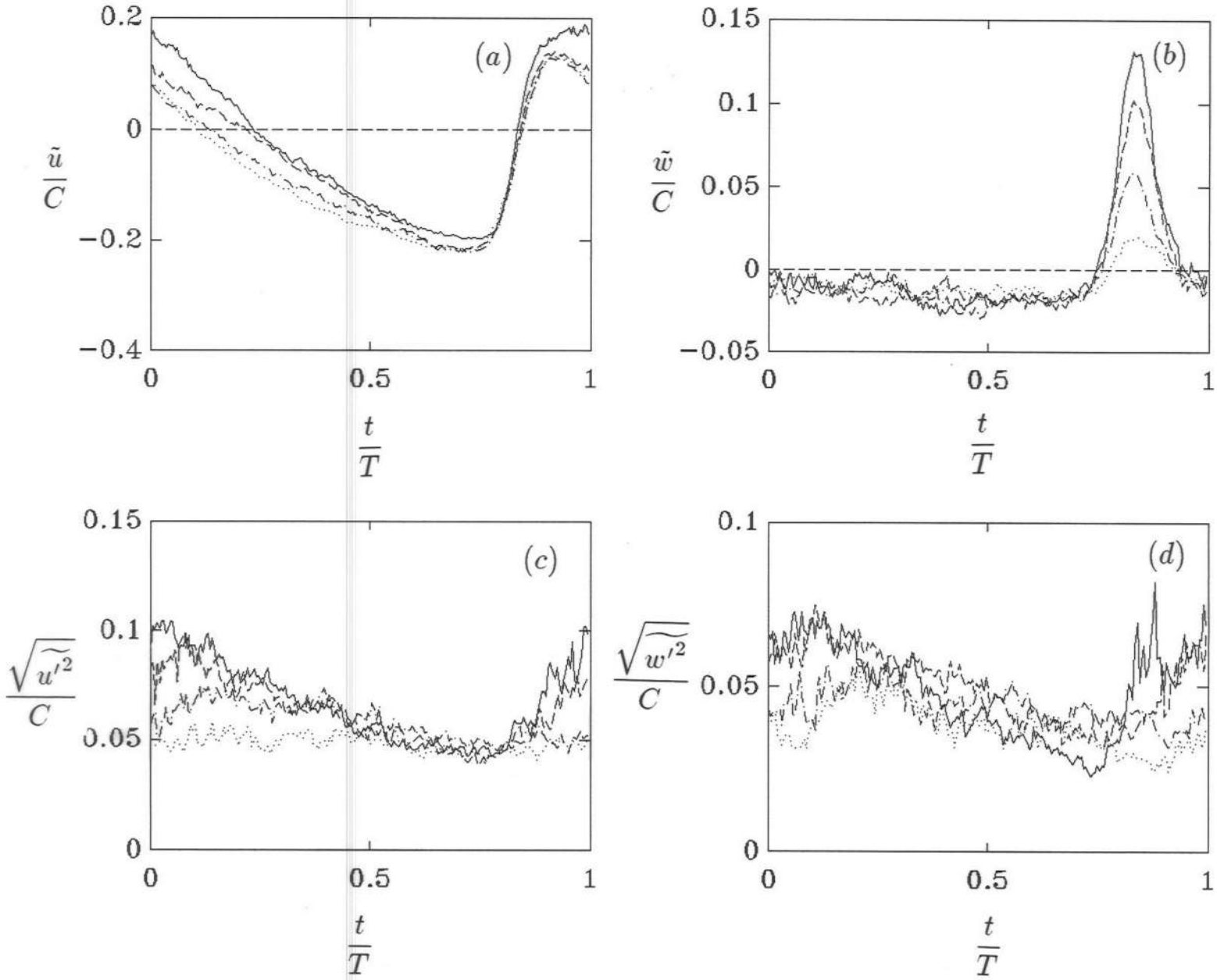
(a)
(b)
(c)
(d)
$\frac{\tilde{u}}{C}$
$\frac{\tilde{w}}{C}$
$\frac{\sqrt{\widetilde{u'^2}}}{C}$
$\frac{\sqrt{\widetilde{w'^2}}}{C}$
$\frac{t}{T}$
0.2
0
−0.2
−0.4
0.15
0.1
0.05
−0.05
0.5
1

FIGURE 6

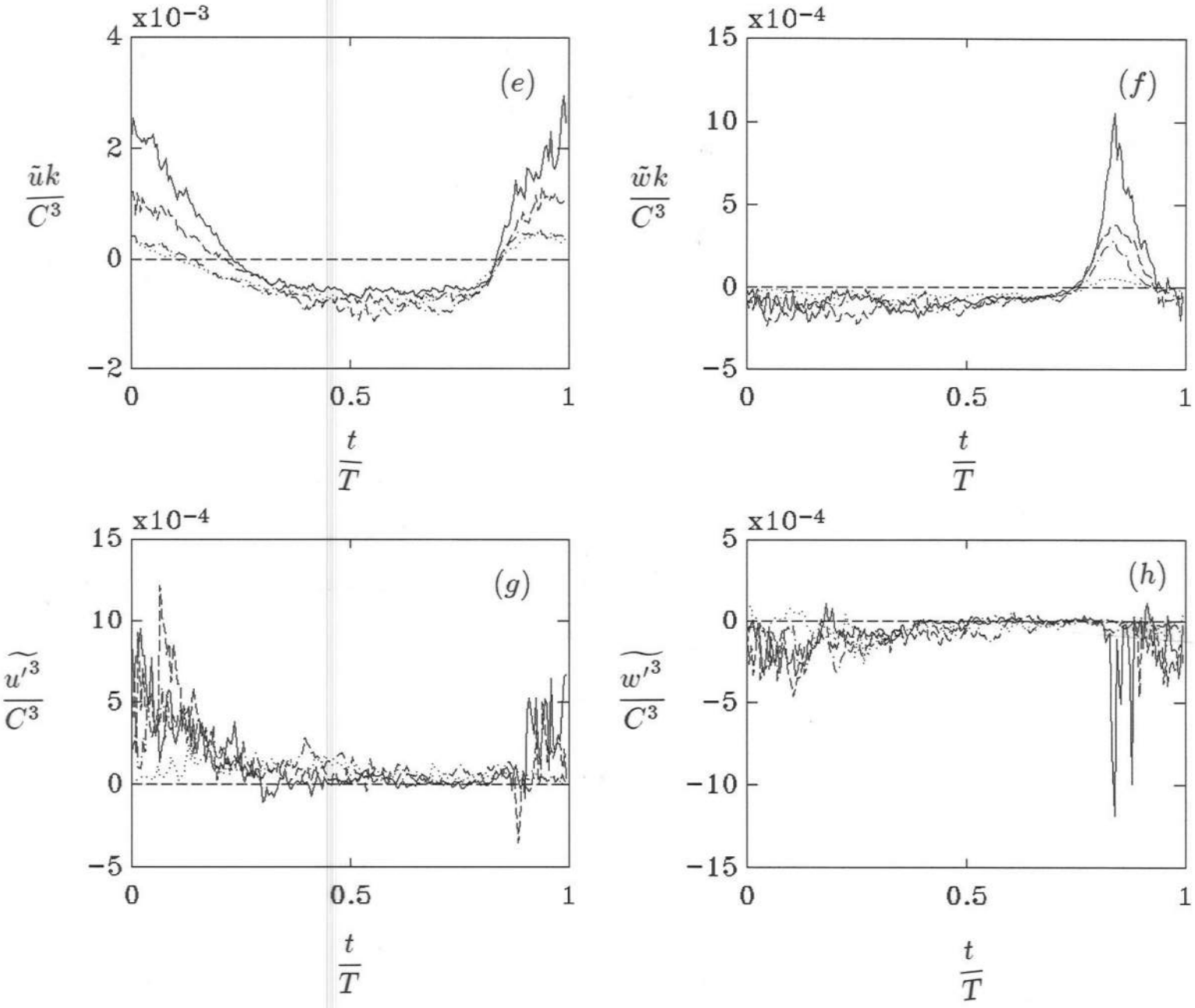


FIGURE 6 (Continued)

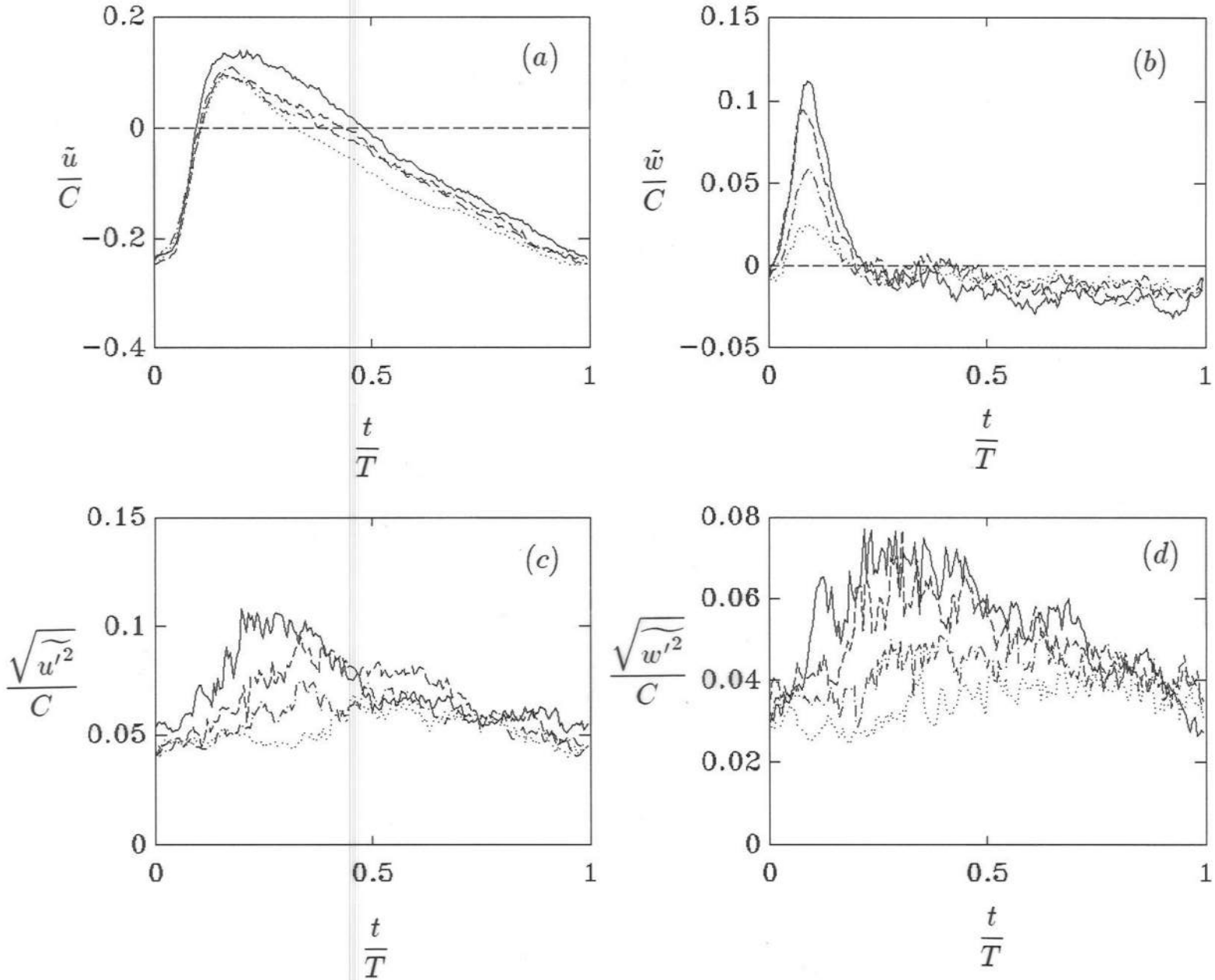
(a)
(b)
(c)
(d)
$\frac{\tilde{u}}{C}$
$\frac{\tilde{w}}{C}$
$\frac{\sqrt{\widetilde{u'^2}}}{C}$
$\frac{\sqrt{\widetilde{w'^2}}}{C}$
$\frac{t}{T}$
0.2
0
−0.2
−0.4
0.15
0.1
0.05
−0.05
0.08
0.06
0.04
0.02
0
0.5
1

FIGURE 7

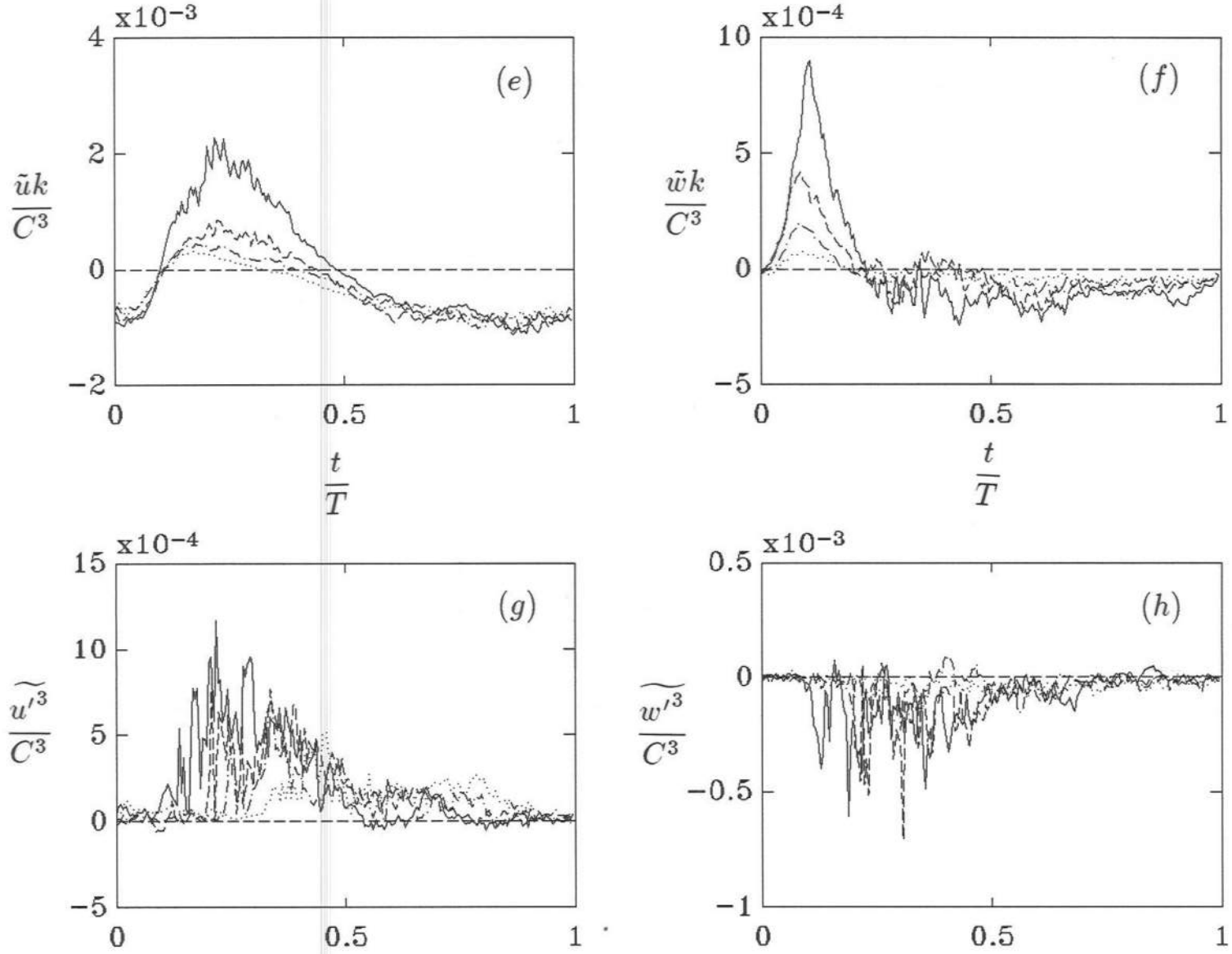


FIGURE 7 (Continued)

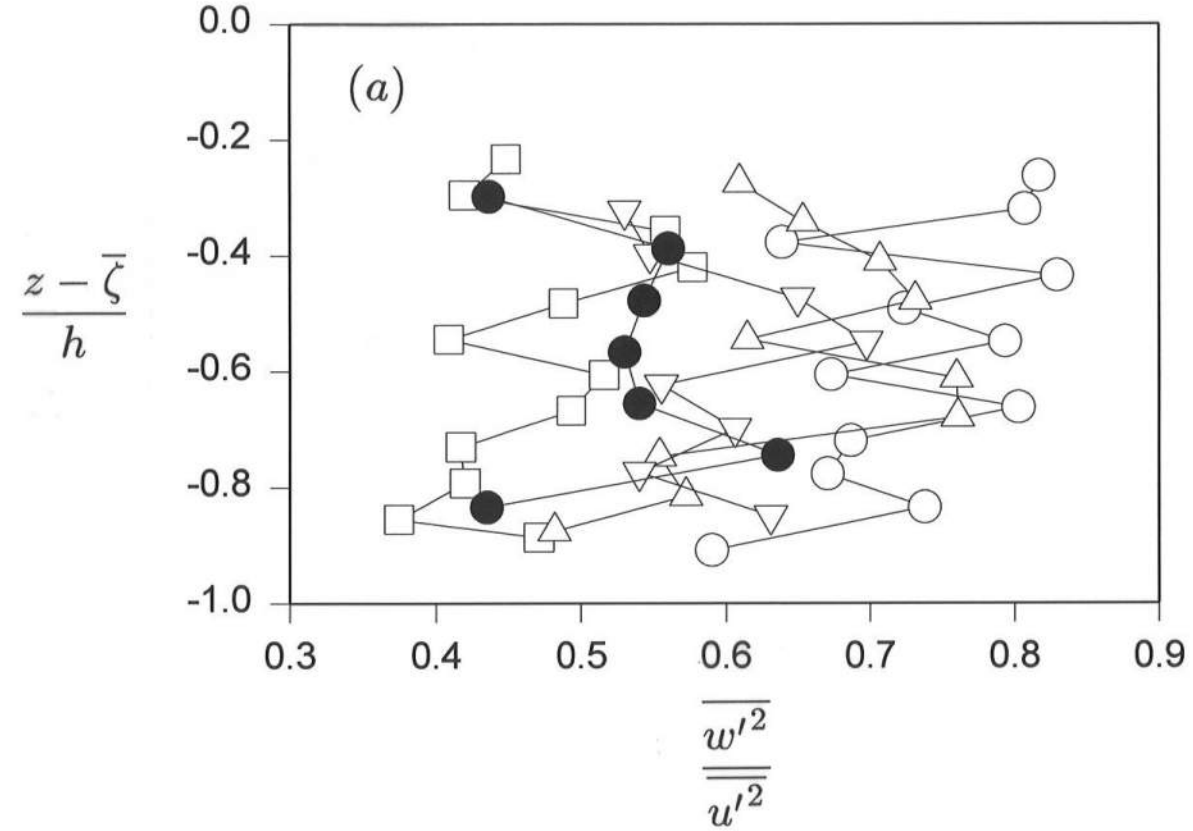
(a)
0.0
-0.2
-0.4
-0.6
-0.8
-1.0
0.3
0.4
0.5
0.6
0.7
0.8
0.9
$\frac{z-\overline{\zeta}}{h}$
$\frac{\overline{w'^2}}{\overline{u'^2}}$

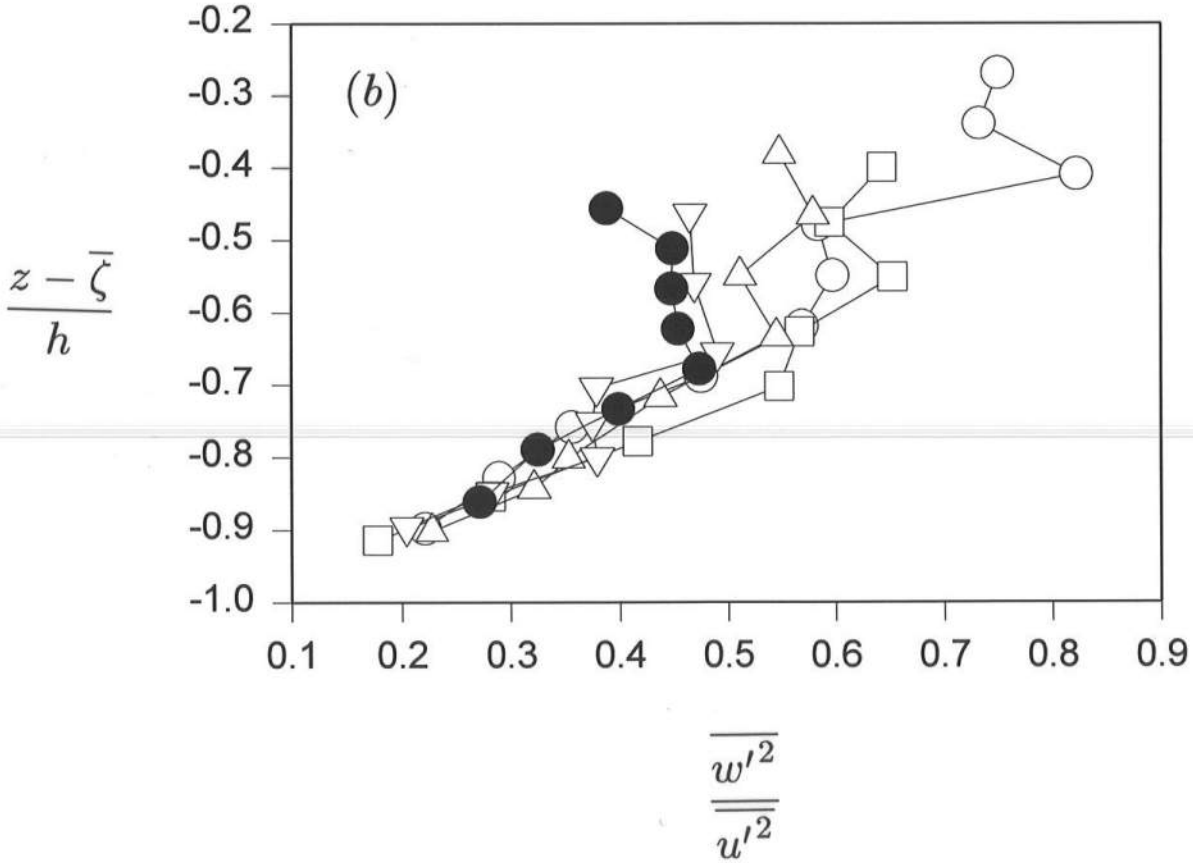
(b)
-0.2
-0.3
-0.4
-0.5
-0.6
-0.7
-0.8
-0.9
-1.0
0.1
0.2
0.3
0.4
0.5
0.6
0.7
0.8
0.9
$\frac{z-\overline{\zeta}}{h}$
$\frac{\overline{w'^2}}{\overline{u'^2}}$

FIGURE 8

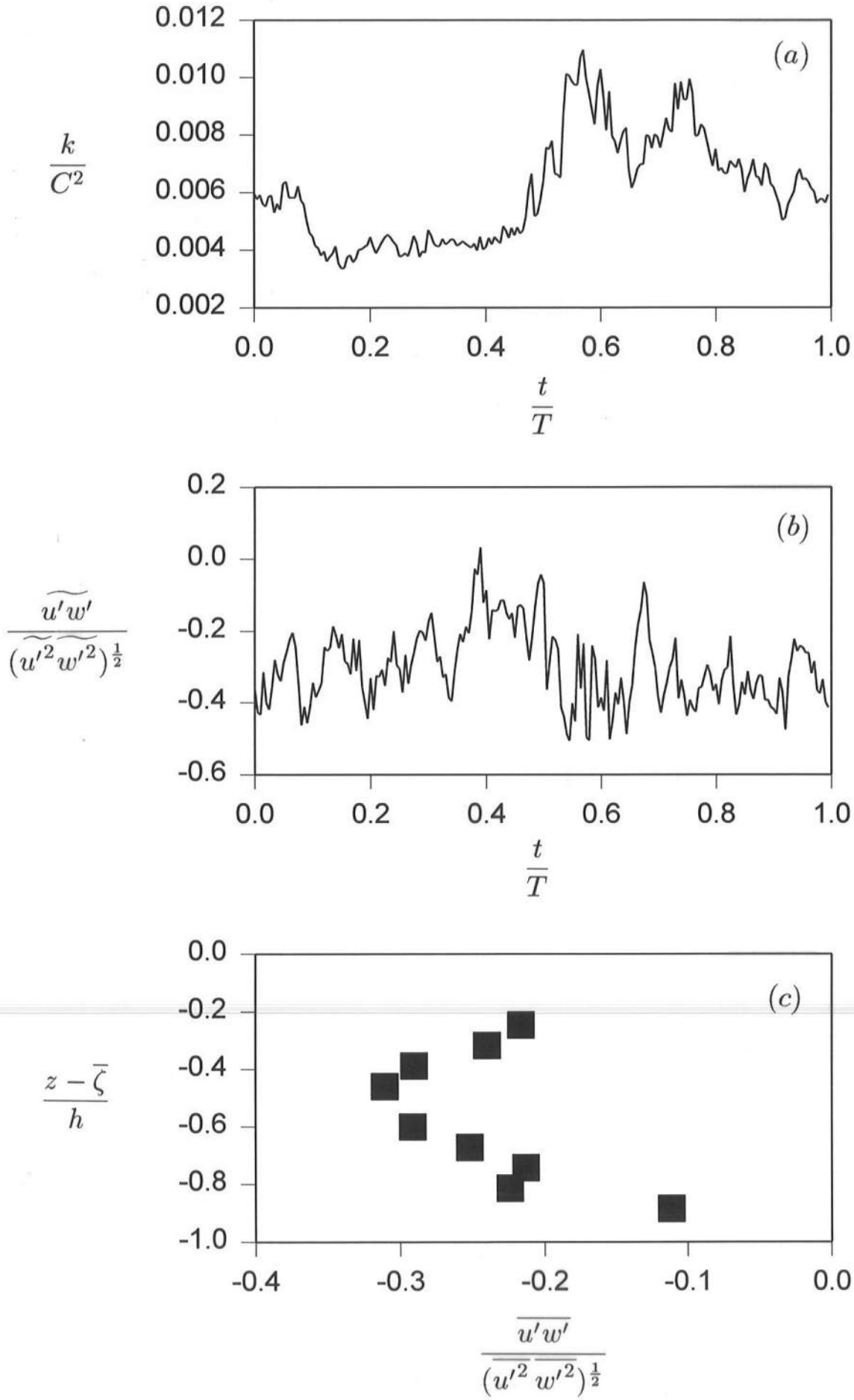
(a)
0.012
0.010
0.008
0.006
0.004
0.002
$\frac{k}{C^2}$
0.0
0.2
0.4
0.6
0.8
1.0
$\frac{t}{T}$
(b)
0.2
0.0
-0.2
-0.4
-0.6
$\frac{\widetilde{u'w'}}{(\widetilde{u'^2}\,\widetilde{w'^2})^{\frac{1}{2}}}$
0.0
0.2
0.4
0.6
0.8
1.0
$\frac{t}{T}$
(c)
0.0
-0.2
-0.4
-0.6
-0.8
-1.0
$\frac{z-\overline{\zeta}}{h}$
-0.4
-0.3
-0.2
-0.1
0.0
$\frac{\overline{u'w'}}{(\overline{u'^2}\,\overline{w'^2})^{\frac{1}{2}}}$

FIGURE 9

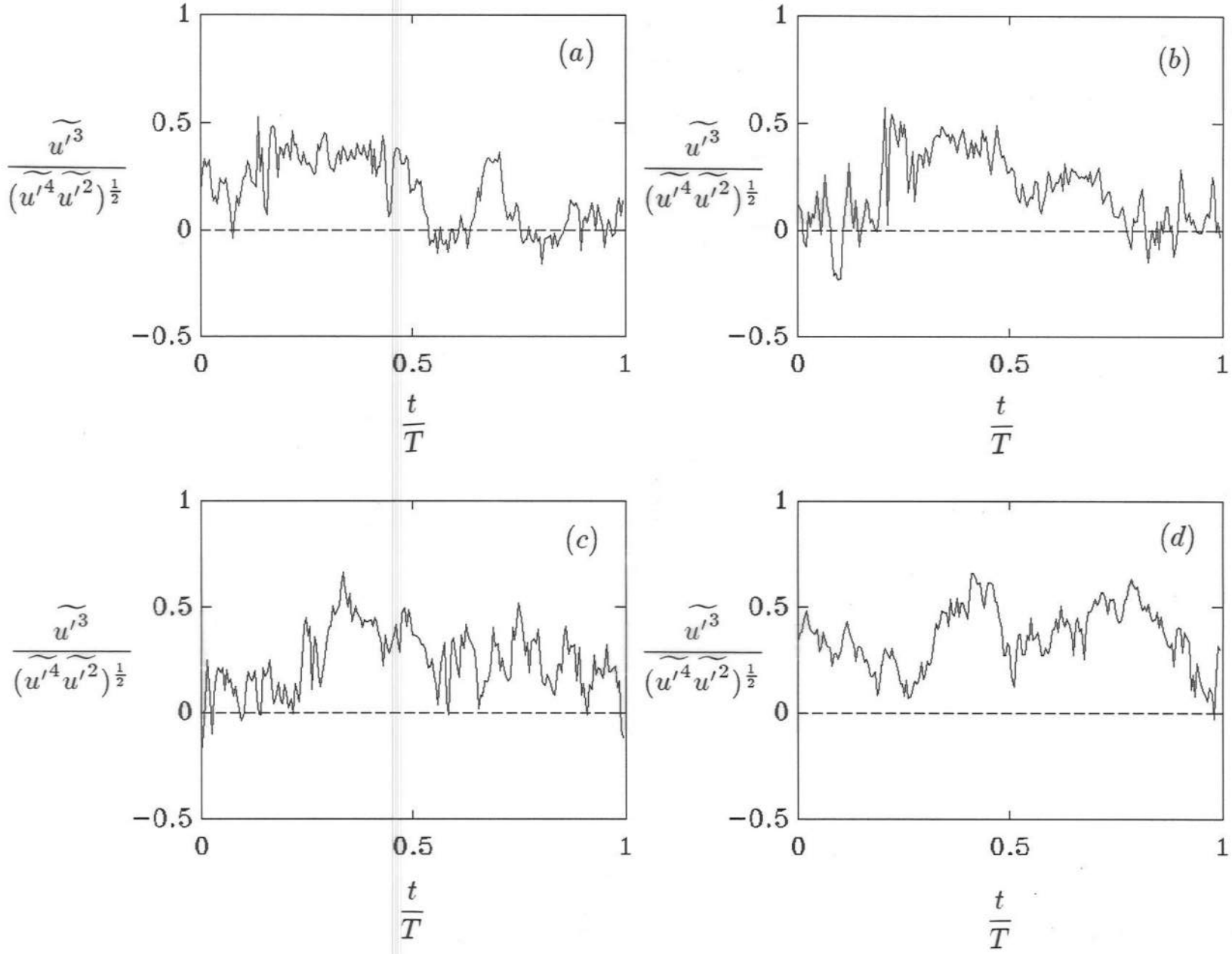
(a)
(b)
(c)
(d)
$\frac{\widetilde{u'^3}}{(\widetilde{u'^4}\widetilde{u'^2})^{\frac{1}{2}}}$
1
0.5
0
−0.5
0
0.5
1
$\frac{t}{T}$

FIGURE 10

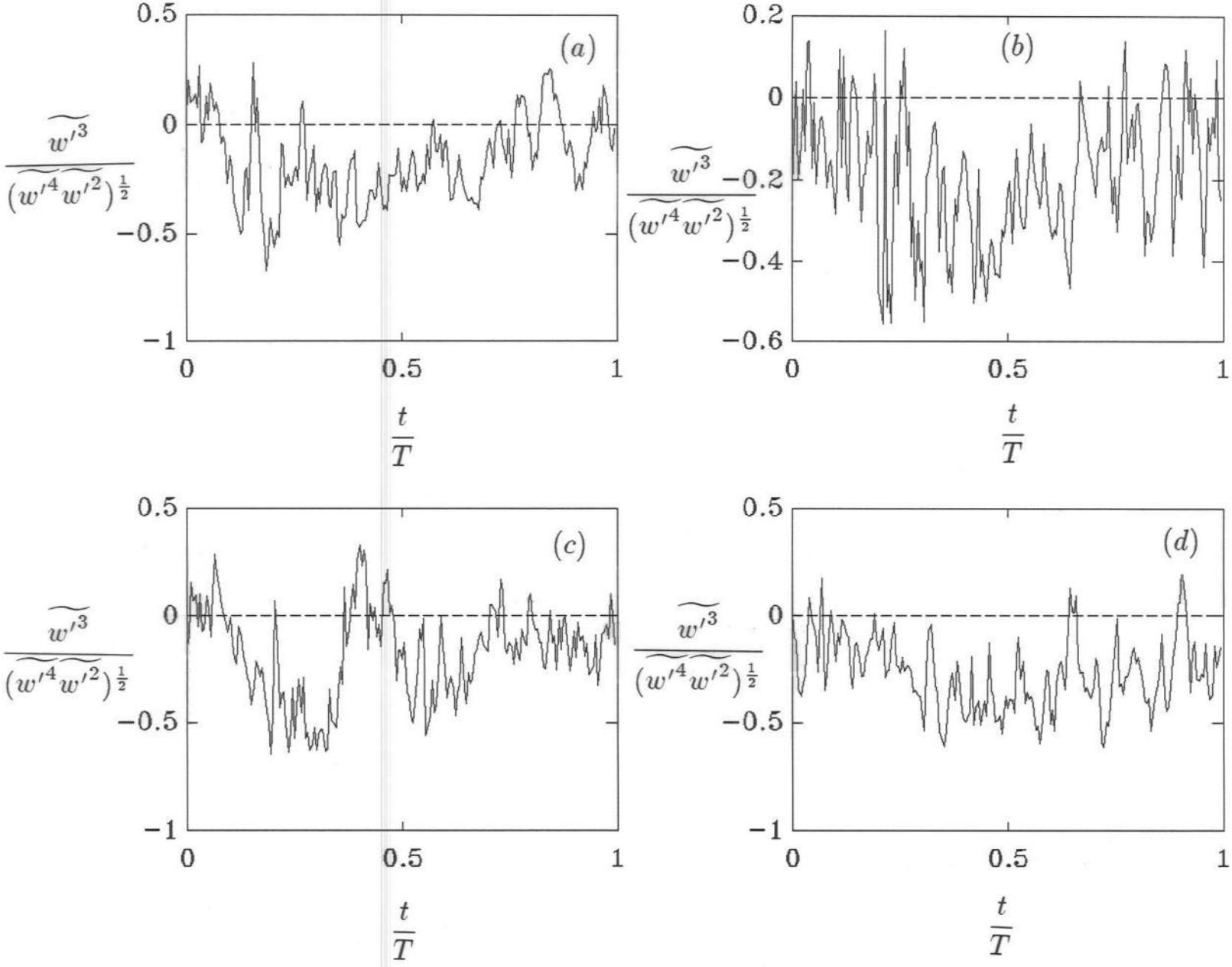
(a)
(b)
(c)
(d)
$\frac{\widetilde{w'^3}}{(\widetilde{w'^4}\widetilde{w'^2})^{\frac{1}{2}}}$
$\frac{t}{T}$
0.5
0
−0.5
−1
0.2
−0.2
−0.4
−0.6
0
0.5
1

FIGURE 11

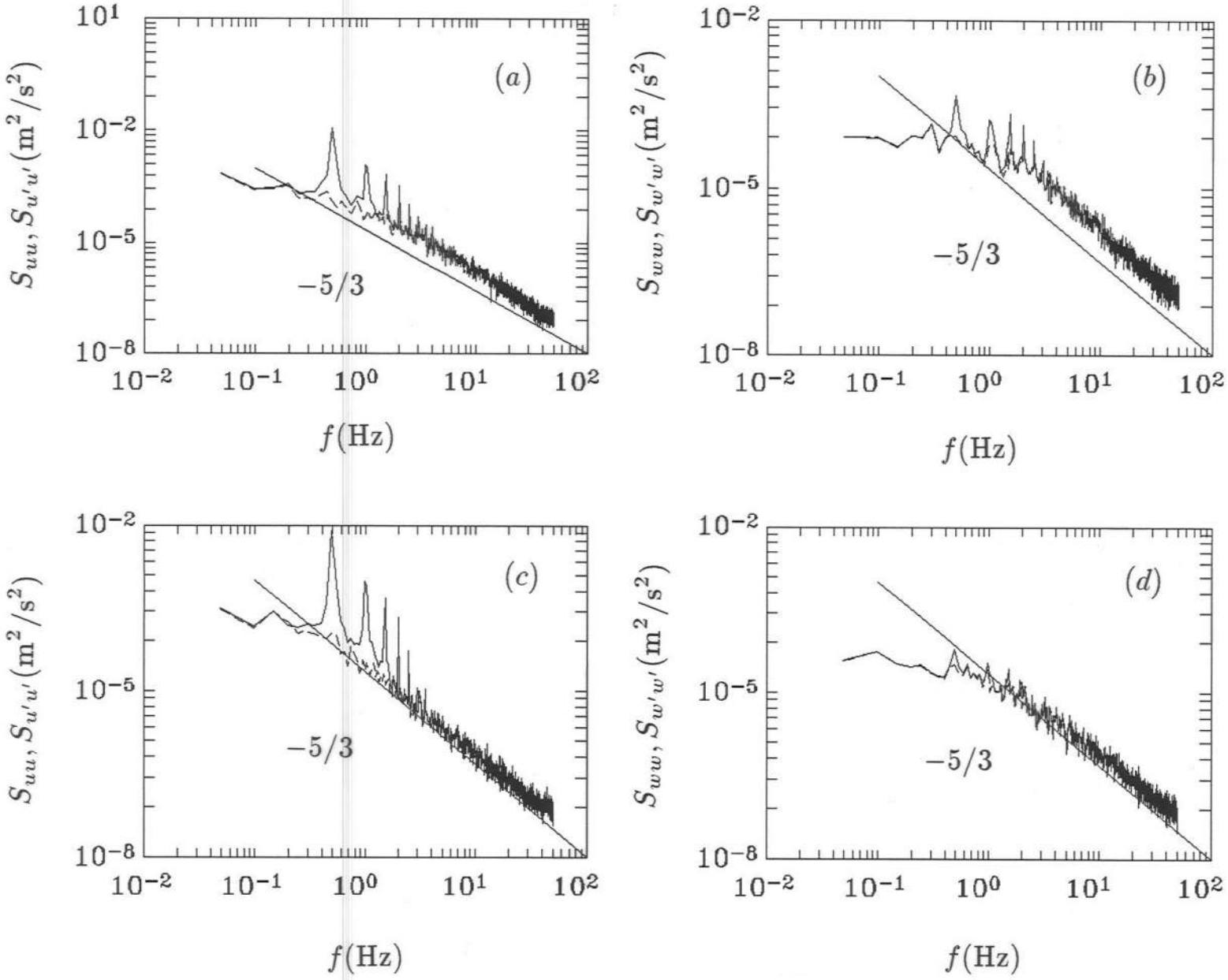
(a)
(b)
(c)
(d)
−5/3
$S_{uu}, S_{u'u'}(\mathrm{m}^2/\mathrm{s}^2)$
$S_{ww}, S_{w'w'}(\mathrm{m}^2/\mathrm{s}^2)$
$f(\mathrm{Hz})$
$10^{1}$
$10^{-2}$
$10^{-5}$
$10^{-8}$
$10^{-2}$
$10^{-1}$
$10^{0}$
$10^{1}$
$10^{2}$

FIGURE 12

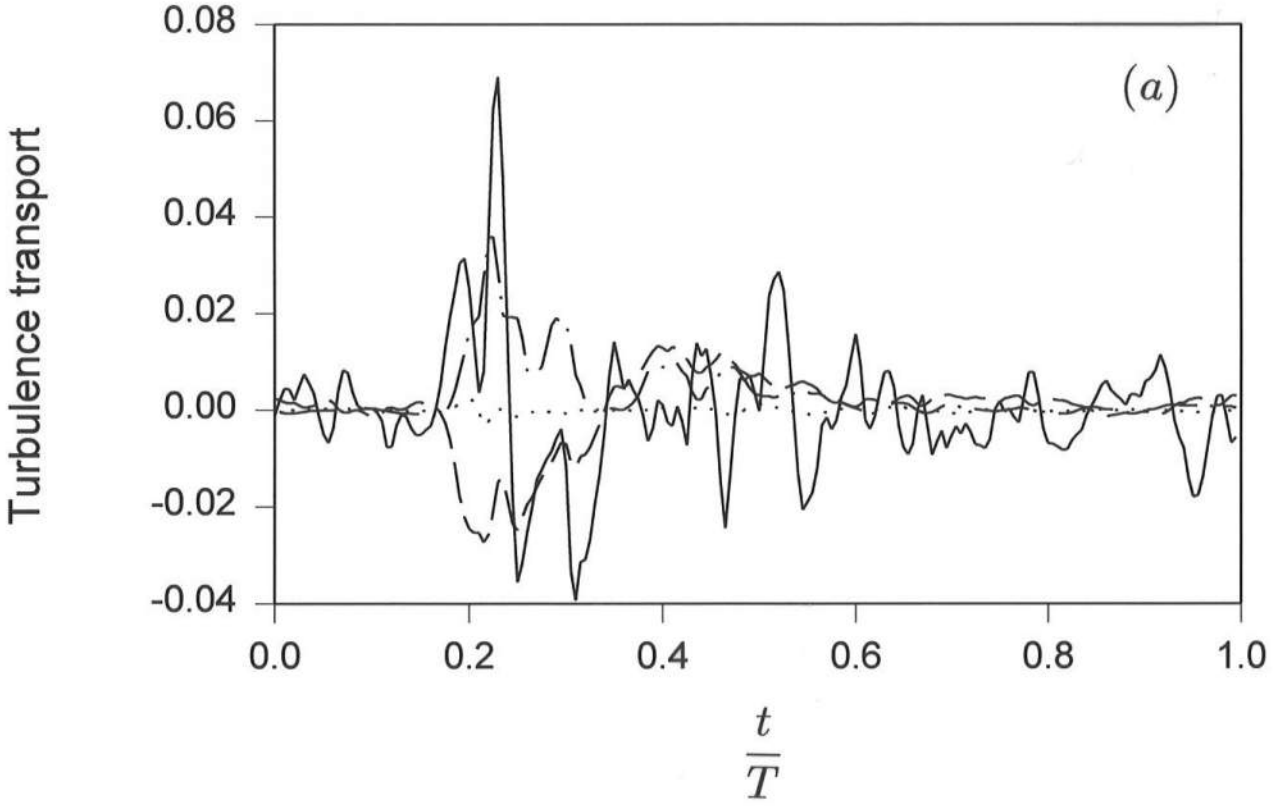
0.08
0.06
0.04
0.02
0.00
-0.02
-0.04
Turbulence transport
(a)
0.0
0.2
0.4
0.6
0.8
1.0
t/T

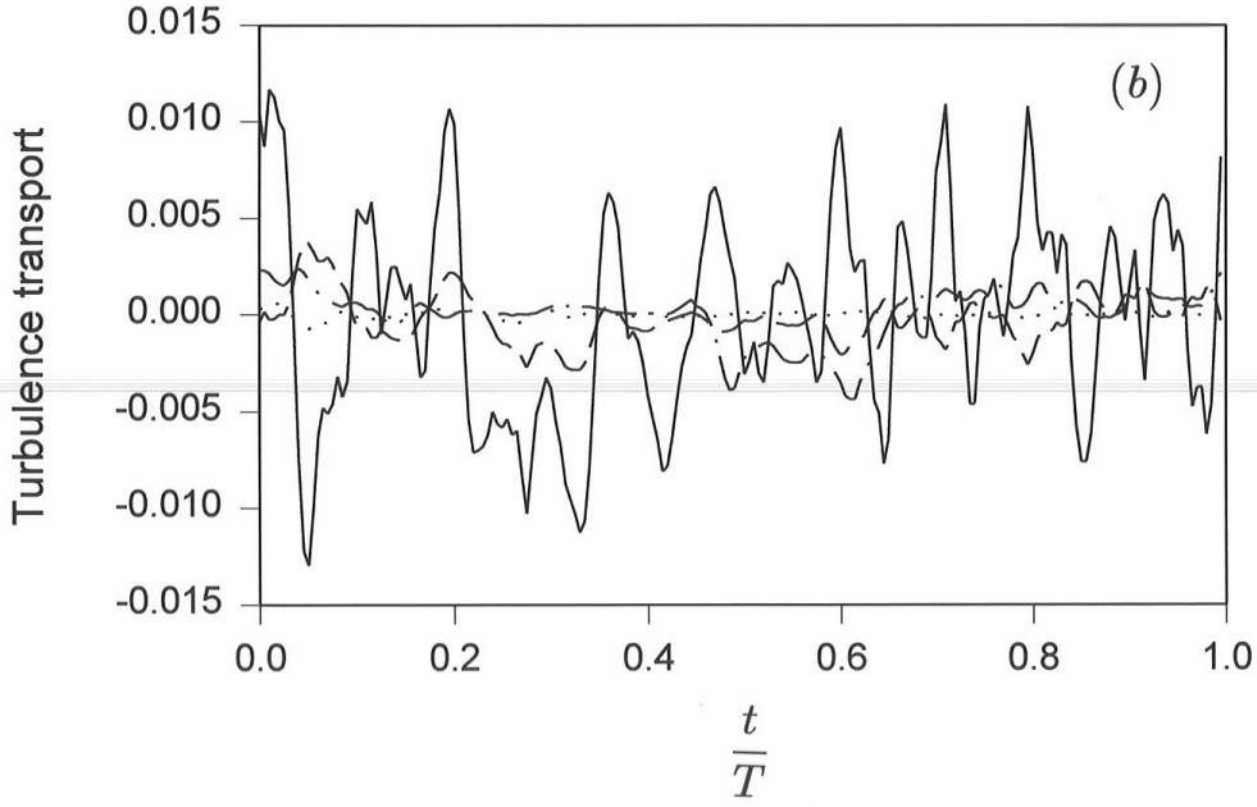
0.015
0.010
0.005
0.000
-0.005
-0.010
-0.015
Turbulence transport
(b)
0.0
0.2
0.4
0.6
0.8
1.0
t/T

FIGURE 13

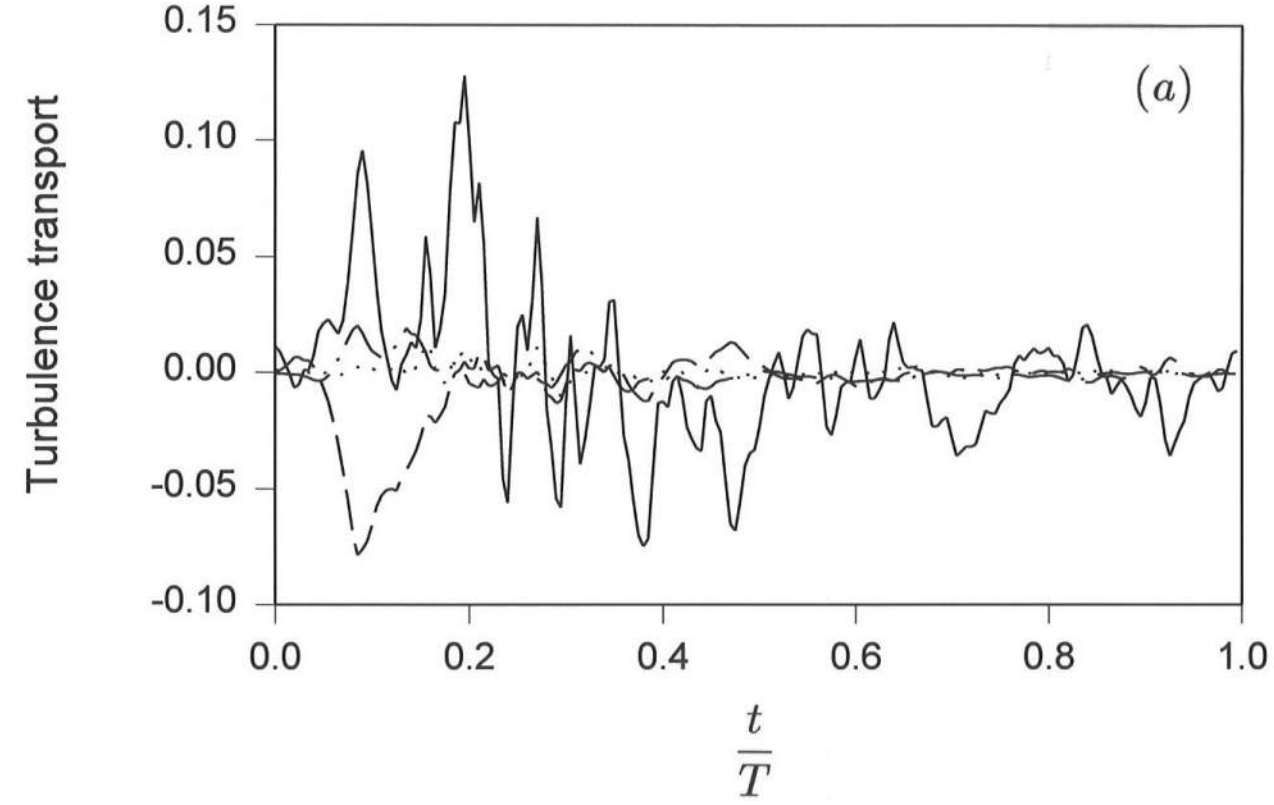
0.15
0.10
0.05
0.00
-0.05
-0.10
Turbulence transport
(a)
0.0
0.2
0.4
0.6
0.8
1.0
$\frac{t}{T}$

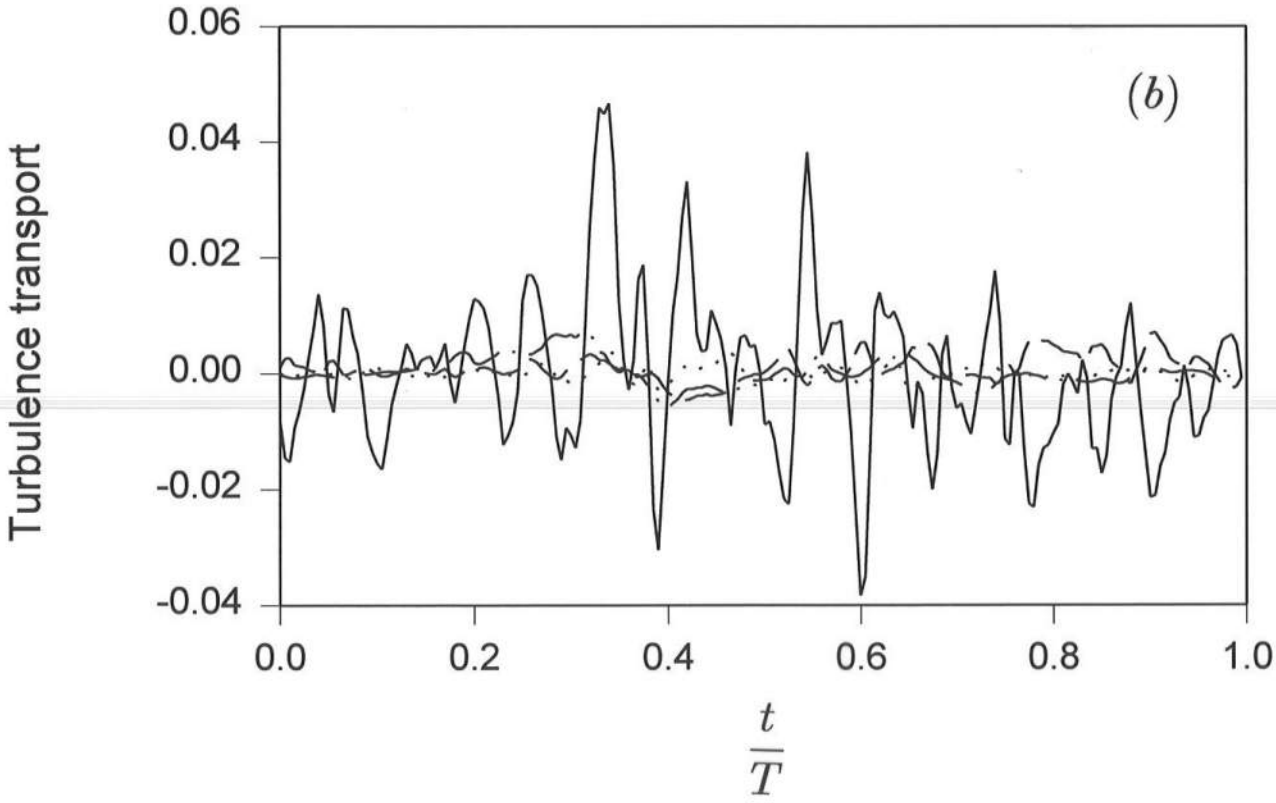
0.06
0.04
0.02
0.00
-0.02
-0.04
Turbulence transport
(b)
0.0
0.2
0.4
0.6
0.8
1.0
$\frac{t}{T}$

FIGURE 14

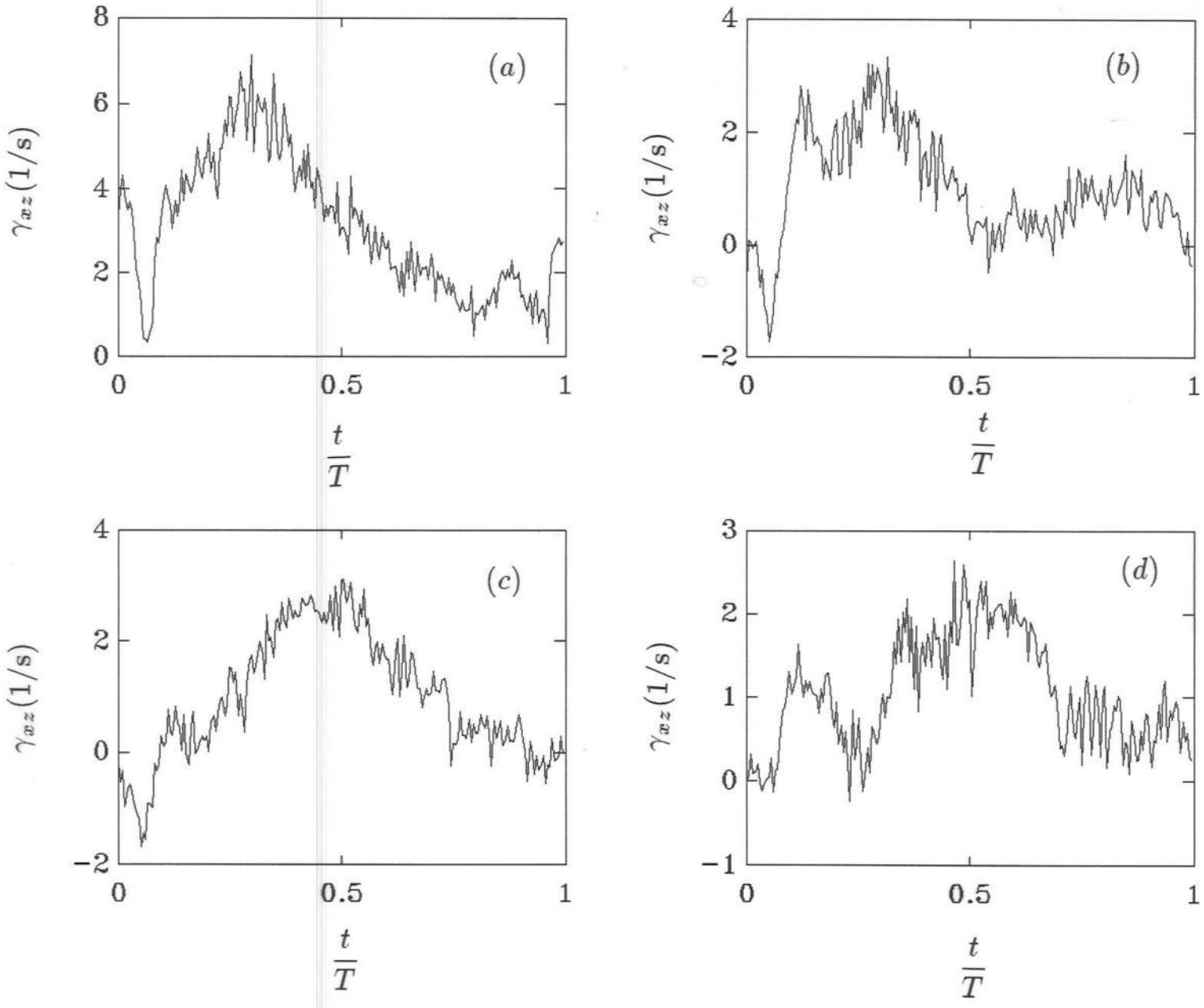


FIGURE 15

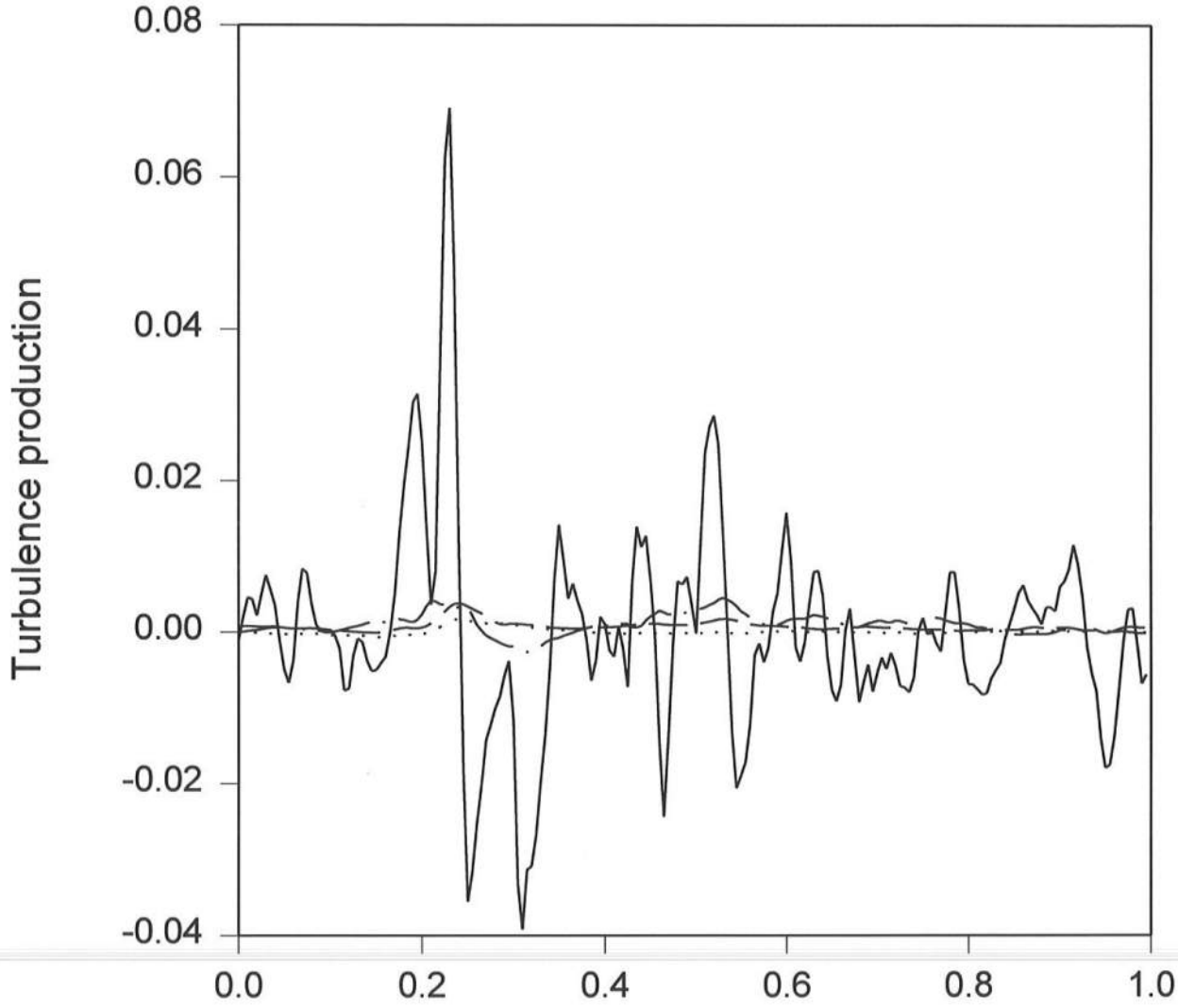
0.08
0.06
0.04
0.02
0.00
-0.02
-0.04
Turbulence production
0.0
0.2
0.4
0.6
0.8
1.0
$\frac{t}{T}$

FIGURE 16

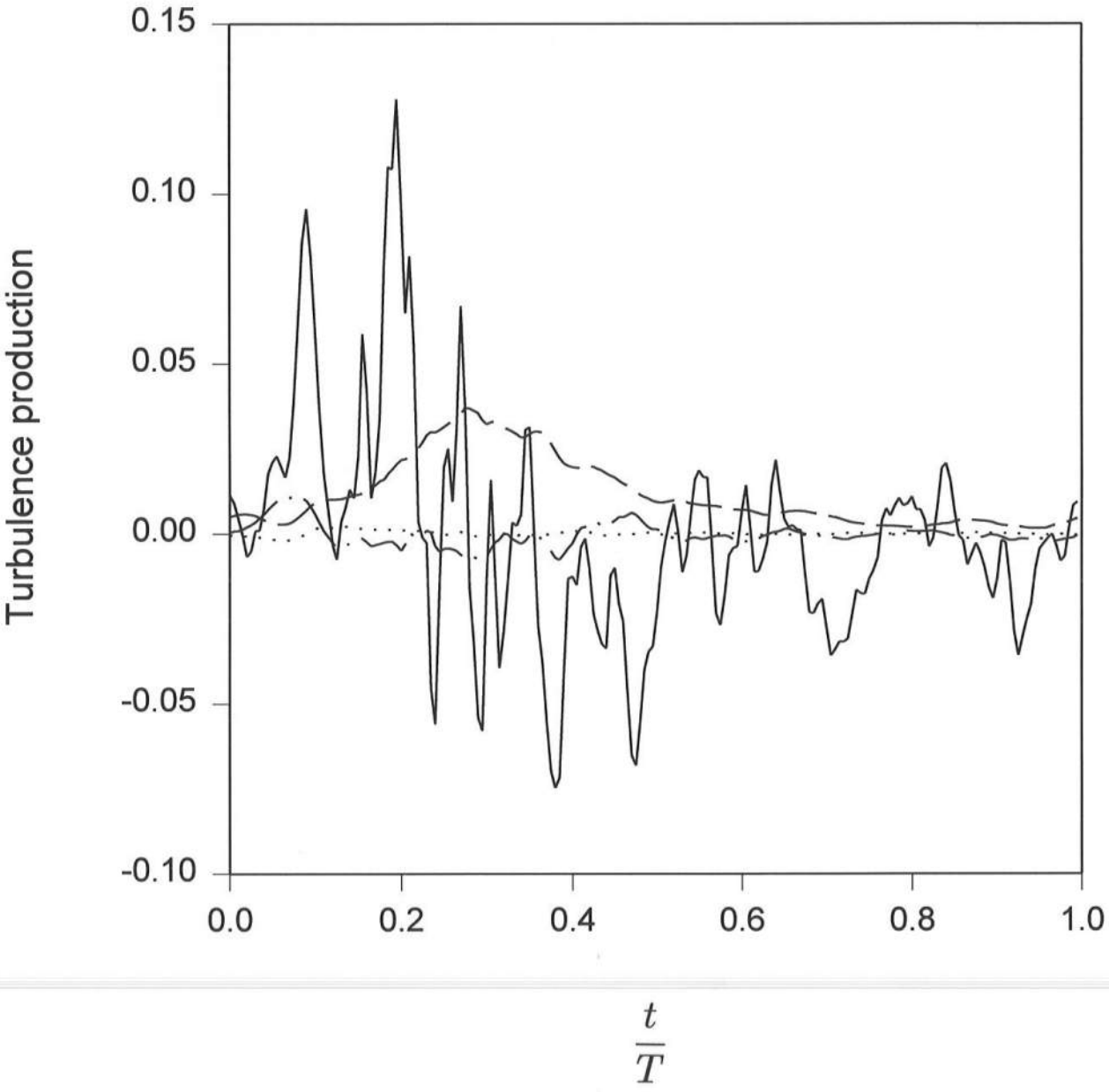
0.15
0.10
0.05
0.00
-0.05
-0.10
Turbulence production
0.0
0.2
0.4
0.6
0.8
1.0
$\frac{t}{T}$

FIGURE 17

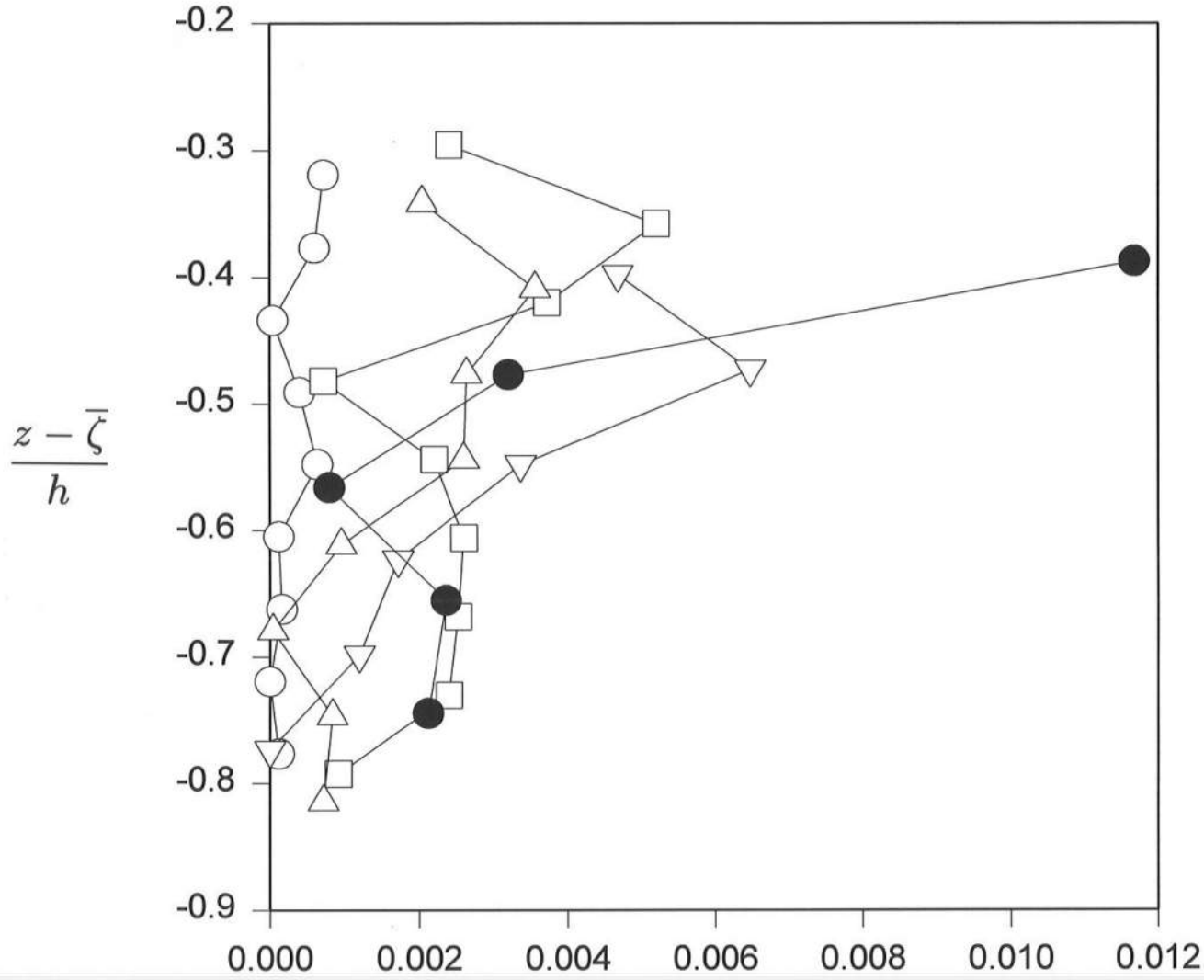
-0.2
-0.3
-0.4
-0.5
-0.6
-0.7
-0.8
-0.9
$\frac{z-\overline{\zeta}}{h}$
0.000
0.002
0.004
0.006
0.008
0.010
0.012
Time-averaged turbulence production

FIGURE 18

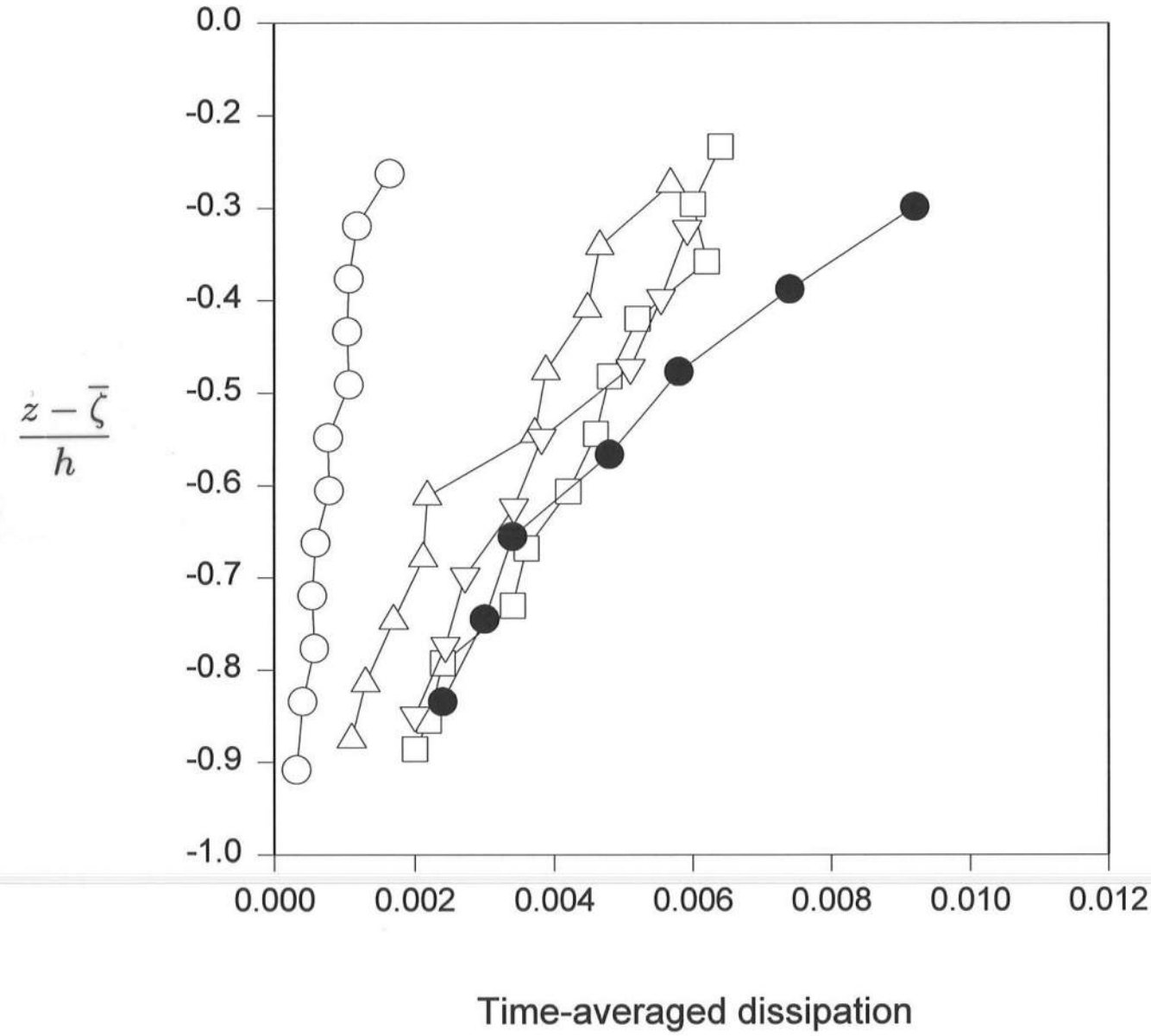
0.0
-0.2
-0.3
-0.4
-0.5
-0.6
-0.7
-0.8
-0.9
-1.0
$\frac{z-\overline{\zeta}}{h}$
0.000
0.002
0.004
0.006
0.008
0.010
0.012
Time-averaged dissipation

FIGURE 19